USGS
science for a changing world

Prepared in cooperation with the National Park Service

Extent of the Last Glacial Maximum (Tioga) Glaciation in Yosemite National Park and Vicinity, California

By Clyde Wahrhaftig, Greg M. Stock, Reba G. McCracken, Peri Sasnett, and Andrew J. Cyr

Pamphlet to accompany
Scientific Investigations Map 3414

2019

U.S. Department of the Interior
U.S. Geological Survey

U.S. Department of the Interior
DAVID BERNHARDT, Secretary

U.S. Geological Survey
James F. Reilly II, Director

U.S. Geological Survey, Reston, Virginia: 2019

Suggested citation:
Wahrhaftig, C., Stock, G.M., McCracken, R.G., Sasnett, P., and Cyr, A.J., 2019, Extent of the Last Glacial Maximum (Tioga) glaciation in Yosemite National Park and vicinity, California: U.S. Geological Survey Scientific Investigations Map 3414, pamphlet 28 p., 1 sheet, scale 1:100,000, 2 appendixes, https://doi.org/10.3133/sim3414.

ISSN 2329-1311 (print)
ISSN 2329-132X (online)
ISBN 978-1-4113-4292-7

Cover. Erratic boulders and glacially scoured granite near Olmsted Point, with Half Dome in distance, Yosemite National Park. Photograph by Kirk Keeler (used with permission).

Preface

Clyde Wahrhaftig (1919–1994) was a geologist whose skills and interests encompassed a broad range of topics, from bedrock geology, to structural geology, to glaciology. Over the course of a long career with the U.S. Geological Survey (USGS) and the University of California, Berkeley (UC Berkeley), Clyde proved to be an exceptional geologist, teacher, and colleague. Geology was more than just a profession for Clyde Wahrhaftig, it was also a passion. An avid hiker and lover of the outdoors, Clyde spent many summers exploring and mapping the geology of Yosemite and the Sierra Nevada, and unraveling the geological complexities of the range became a labor of love.

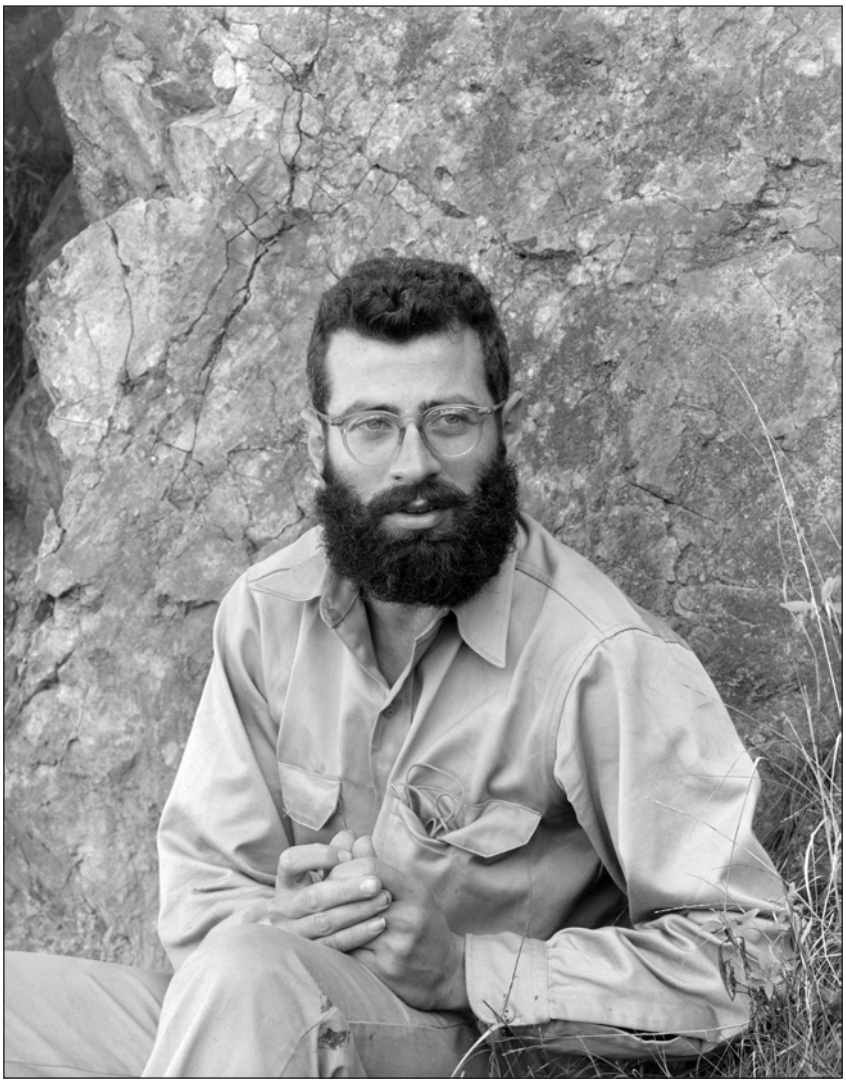

Clyde Wahrhaftig in the field in 1952. Photograph by Imogen Cunningham.

Clyde began formally working on a map of the Last Glacial Maximum (Tioga-age) glacier extent in Yosemite National Park in the early 1980s, but this work was built on observations he had made over a much longer period. Clearly, he was thinking about glaciation while working on the geologic map of the Tower Peak quadrangle in northeastern Yosemite (Wahrhaftig, 2000), which he began in 1955, as his pioneering mapping of boulder trains there revealed the subtle ice-flow patterns in that region. He also incorporated glacier mapping into his UC Berkeley field geology courses, having his students map striations and other glacier flow indicators. In the early 1980s, with funding from the USGS, Clyde began a focused effort to map the extent of glacial ice in and around Yosemite National Park during the Tioga glaciation. Along with USGS colleagues Malcolm Clark and N. King Huber, Clyde dedicated several summers to mapping glacial features. Clyde often planned his field excursions to coincide with National Park Service (NPS) trail-crew encampments, which offered trail workers opportunities to learn about Yosemite geology in return for Clyde's joining the trail crew for dinner.

The USGS published a preliminary version of the Yosemite glacier map in 1987 (Alpha and others, 1987) to accompany a comprehensive update on the geology of Yosemite written by N. King Huber (1987). This early version consisted of an oblique view of the Tioga-age ice extent in and around Yosemite National Park, painstakingly hand drawn by cartographer Tau Rho Alpha. The map showed many of the key details related to the Tioga glaciation, but it lacked the plan-view perspective needed to fully depict the ice extent, thickness, and flow directions. Much to Clyde's dismay, the map also included some errors, as noted in a subsequent erratum (see https://pubs.usgs.gov/imap/i1885/). Clyde always intended to publish a comprehensive plan-view version of the glacier map that would correct these errors, include additional details lacking in the oblique-view map, and present the data upon which the map was based. However, he felt that more work was needed. This was undoubtedly correct, but it may also have been that Clyde was reluctant to finish a project that brought him so much joy.

Unfortunately, increasing heart problems gradually limited Clyde's ability to work at high elevation, and though he worked diligently until his death in 1994, he did not complete the plan-view glacier map to his demanding standards. Knowing that he would not finish the map, Clyde left an allowance in his will for others to do so. Those trust funds were eventually granted to this report's second author in 2006, as the first park geologist employed by the NPS at Yosemite. Twenty-five years after Clyde's death, and including more than a decade of our own work, the map is finally completed and published. As Clyde's coauthors, we share his feeling that more work is needed (and also his reluctance to conclude such a joyful project), but we also recognize that an effort of this magnitude will never be perfect. It is time to share this work and let future researchers improve upon it.

It has been an interesting experience to collaborate with a colleague who is deceased, and whom we never even had the opportunity to meet. Fortunately, Clyde made this collaboration easy by generating very detailed field maps at the 15-minute scale, taking thorough notes with sketches of his field observations, and writing a preliminary version of this pamphlet. Clyde's colleagues and students helped to fill in some of the gaps by offering suggestions for interpretation, providing important historical background, and sharing many revealing anecdotes about Clyde's wonderfully idiosyncratic personality. We were further encouraged by examples in which researchers' work in Yosemite, including that of Clyde Wahrhaftig, was published posthumously by their colleagues (see, for example, Matthes, 1950; Calkins and others, 1985; Wahrhaftig, 2000).

Using the funds provided by Clyde's trust, we have given his preliminary map a thorough and critical review. We field-checked many key sites, including some not visited by Clyde, and measured additional ice-flow indicators. We also incorporated many new techniques, such as lidar (light detection and ranging)-based mapping of glacial features and terrestrial cosmogenic-nuclide-exposure dating of moraine boulders and erratics, techniques that were not available to Clyde but which he no doubt would have enthusiastically embraced. Yet, for all of the additional work and newly available techniques, the final map published here is not substantially different from Clyde's initial draft. With the application of each new technique or the discovery of each new piece of evidence, we were reminded of how well Clyde understood the glacial processes that shaped Yosemite and how intimately connected he was with these landscapes. Although we have contributed in various ways, fundamentally this map is the result of decades of devoted work by Clyde Wahrhaftig. We feel privileged to have engaged in this collaboration, even posthumously, and we hope that you enjoy learning from Clyde as much as we have.

Evening light on glacially sculpted peaks south of Tuolumne Meadows. During the Last Glacial Maximum (Tioga) glaciation, these sharp peaks projected above the great Tuolumne icefield. Photograph by Ryan Alonzo (used with permission).

Acknowledgments

King Huber and Malcolm Clark of U.S. Geological Survey (USGS) conducted field observations that contributed to this map. We thank Lupin Amstutz, Nikita Avdievitch, Laura Clor, Camille Collett, Taylor Kenyon, Megan Mason, Marianne Okal, Roger Putnam, Heather Rogers, Autumn Stock, and Sarah Stock for field assistance. We also thank Laura Clor, Taylor Kenyon, Mariah Radue, and Keenan Takahashi (all National Park Service [NPS]) for drafting assistance. Airborne lidar data were provided by Thomas Painter and Kathryn Bormann of the National Aeronautics and Space Administration Airborne Snow Observatory, and by the Center for Airborne Laser Mapping. Cosmogenic ^{10}Be analyses were performed at the PRIME lab at Purdue University and at the Center for Accelerator Mass Spectrometry at Lawrence Livermore National Laboratory. Reba McCracken and Peri Sasnett were supported by NPS's Geoscientist-in-the-Parks program. We appreciate discussions with, and assistance from, Malcolm Clark, Wes Hildreth, King Huber, Angela Jayko, and Jan van Wagtendonk (all USGS); Guleed Ali (Columbia University); Robert Anderson and Mark Kessler (both University of Colorado, Boulder); Richard Becker (University of Wisconsin); Doug Clark (Western Washington University); Kurt Cuffey and Doris Sloan (both University of California, Berkeley); Connie Millar (U.S. Forest Service); Fred Phillips (New Mexico Tech); Jeffrey Schaffer (Napa Valley College); and Scott Stine (California State University, East Bay). James Moore (USGS), Kurt Cuffey, Doug Clark, and Scott Stine provided helpful reviews. The Trust of Clyde Wahrhaftig funded this research, and we thank Jack Wahrhaftig and Doris Lindheim for their generous support. All photographs (unless otherwise noted) were taken by Greg Stock.

Contents

Figures

Tables

Conversion Factors

U.S. customary units to International System of Units

Multiply	By	To obtain
	Length	
inch (in.)	2.54	centimeter (cm)
foot (ft)	0.3048	meter (m)
mile (mi)	1.609	kilometer (km)
	Area	
square foot (ft^2)	0.09290	square meter (m^2)
square mile (mi^2)	2.590	square kilometer (km^2)
	Volume	
cubic inch (in^3)	16.39	cubic centimeter (cm^3)
cubic foot (ft^3)	0.02832	cubic meter (m^3)
cubic mile (mi^3)	4.168	cubic kilometer (km^3)
	Mass	
ounce, avoirdupois (oz)	28.35	gram (g)
ounce, avoirdupois (oz)	2,835.0	milligram (mg)
	Density	
pound per cubic foot (lb/ft^3)	0.01602	gram per cubic centimeter (g/cm^3)

Abbreviations

amsl	above mean sea level
Be	beryllium
^{9}Be	beryllium-9
^{10}Be	beryllium-10
CAMS	Center for Accelerator Mass Spectrometry
CRONUS	Cosmic-Ray Produced Nuclide Systematics
cm	centimeter(s)
cm/yr	centimeters per year
DEM	digital elevation model
E	east
g	gram(s)
g^{-1}	per gram

g/cm^3	gram(s) per cubic centimeter
GPS	global positioning system
ka	thousand years old
km	kilometer(s)
m	meter(s)
mg	milligram(s)
N	north
NAD83	North American Datum 1983
NPS	National Park Service
PRIME	Purdue Rare Isotope Measurement
SiO_2	silicon dioxide
UC Berkeley	University of California, Berkeley
USGS	U.S. Geological Survey
UTM	Universal Transverse Mercator
yr	year(s)
yr^{-1}	per year

Extent of the Last Glacial Maximum (Tioga) Glaciation in Yosemite National Park and Vicinity, California

By Clyde Wahrhaftig,[1,2*] Greg M. Stock,[3] Reba G. McCracken,[3] Peri Sasnett,[3] and Andrew J. Cyr[1]

Introduction

Yosemite National Park, located in the central Sierra Nevada in California, is an icon of the U.S. National Park system, famous for its many spectacular geologic features. These features include the towering cliffs and hanging waterfalls of Yosemite Valley, and the rounded granite domes, deep blue lakes, and jagged peaks and spires of the high country. More subtle but just as spectacular are the vast areas of polished granite, linear scratches, and isolated boulders scattered across the landscape. All of these features owe their origin, at least in part, to glaciers.

Glaciers originating at the crest of the Sierra Nevada flowed down preexisting river canyons numerous times throughout the Quaternary Period (the past 2.6 million years) (Matthes, 1929; Blackwelder, 1931). Although the field evidence for past glaciations is necessarily incomplete (Gibbons and others, 1984), at least seven distinct glacial periods have been identified in the Sierra Nevada, spanning a minimum of 1.5 million years (table 1; see also, Blackwelder, 1931; Sharp and Birman, 1963; Birman, 1964; Fullerton, 1986; Gillespie and Clark, 2011).

The map shows the extent of alpine icefields and associated valley glaciers in Yosemite National Park and vicinity during the most recent large glaciation, known as the Last Glacial Maximum. The Last Glacial Maximum is a globally recognized cold period characterized by low sea levels and the growth of ice sheets and mountain glaciers (Clark and others, 2009). In the Sierra Nevada, the Last Glacial Maximum glaciation is referred to as the Tioga glaciation (Blackwelder, 1931). At least four glaciations that occurred prior to the Tioga glaciation (table 1) were larger in extent (Blackwelder, 1931; Sharp and Birman, 1963; Birman, 1964; Fullerton, 1986; Gillespie and Clark, 2011). However, by virtue of being the most recent of the large Pleistocene glaciations, the evidence for the Tioga glaciation is abundant and relatively well preserved in the Yosemite landscape. The Tioga glaciation likely involved at least two, and perhaps as many as four, major glacial advances spanning the interval from approximately 27,000 to 15,000 years ago; the largest of these, representing the maximum ice extent shown on the map, occurred from approximately 21,000 to 18,000 years ago (see, for example, Benson and others, 1998; Bischoff and Cummins, 2001; Phillips and others, 2009; Rood and others, 2011; Phillips, 2016, 2017). Although it is possible that the various Tioga-age glaciers in the study area attained their maximum extents at slightly different times during the Last Glacial Maximum, for the purposes of this map we assume that they reached their maximum extents simultaneously. The maximum ice extent shown here may have occupied certain areas only briefly.

During the maximum extent of the Tioga glaciation, glaciers and ice fields covered most areas in and around Yosemite National Park above 2,700 meters (m) elevation. Glaciers in the map area occupied six major drainage basins: the Tuolumne, Merced, and San Joaquin River basins on the western slope of the Sierra Nevada, and, on the eastern slope, basins of the Walker and Owens Rivers and Mono Lake. Glaciers draining westward from the Sierra crest were approximately seven times longer than those draining eastward, owing to the strong topographic asymmetry of the mountain range and the resulting strong rainshadow effect (Kessler and others, 2006). In some places, the Tioga-age ice divide was as much as 2.5 kilometers (km) west of the present drainage divide along the Sierra crest, allowing ice from the interior of the range to flow up and over the crest into eastward-draining canyons. As a result, many of the passes along the crest of the Sierra Nevada are remarkably wide and gentle; a notable example is Peeler Lake, a large lake situated on the crest that has two outlets, one draining to the Great Basin on the east and the other to the Pacific Ocean on the west.

On the western slope of the Sierra Nevada, Tioga-age glaciers extended tens of kilometers down the major river canyons. The largest of these was the Tuolumne glacier, which flowed for a distance of nearly 80 km from its source at Mount Lyell, down the Grand Canyon of the Tuolumne River and through Hetch Hetchy Valley, to a terminus at approximately 640 m elevation. The maximum ice thickness in the region was in the Grand Canyon of the Tuolumne River near Harden Lake, where the glacier was nearly 1,200 m thick. Smaller valley glaciers flowed down the canyon of the Merced River to a terminus at approximately 1,190 m elevation, near Bridalveil Meadow in Yosemite Valley, as well as down the South Fork Merced River to a terminus at

[1]U.S. Geological Survey.

[2]University of California, Berkeley.

[3]National Park Service, Yosemite National Park.

[*]Deceased

Table 1. Recognized glaciations in the Sierra Nevada and their approximate ages.

Glaciation	Approximate age, in thousands of years ago	Age references
Matthes (Little Ice Age)	0.6–0.15	Wood (1977); Stine (1994)
Recess Peak	14–12.5	Clark and Gillespie (1997); Clark and others (2003); Phillips and others (2009); Phillips (2016, 2017)
Tioga (Last Glacial Maximum)	27–15	Phillips and others (1996, 2009); James and others (2002); Rood and others (2011); Phillips (2016, 2017)
Tahoe	145–130	Rood and others (2011); Phillips (2016, 2017); Hildreth and Fierstein (2016)
Mono Basin	160–60	Sharp and Birman (1963); Phillips and others (1990)
Sherwin	900–790	Sharp (1968); Birkeland and others (1980); Nishiizumi and others (1989)
McGee	~2,600–1,500	Dalrymple (1963, 1964); Huber (1981)

approximately 1,250 m elevation near Wawona. Valley glaciers extended down the canyons of the various forks of the San Joaquin River, coalescing in the vicinity of Balloon Dome and terminating at an elevation of approximately 1,100 m.

Some of the ice filling the basin of the Lyell Fork (of the Tuolumne River) spilled over low passes in the Cathedral Range to augment ice in the upper Merced River drainage. Glacier ice also flowed over a pass southwest of Tuolumne Meadows and down Tenaya Canyon to join the Merced glacier in eastern Yosemite Valley. In most cases the major ice streams converged in the downslope direction, such as in the Grand Canyon of the Tuolumne River, but, at some locations, ice streams diverged around peaks or over passes, such as east of Mount Lyell near Thousand Island Lake, and at Reversed Peak near June Lake.

On the eastern slope of the Sierra, glaciers cascaded down smaller canyons cut into the steep eastern escarpment. Glaciers on the eastern slope terminated at higher elevations than their western counterparts because of their smaller drainage basin areas and a more arid environment east of the Sierra crest. Glacier terminus positions in the Mono Basin (southeast of Mono Lake, just east of the map area) are found above an elevation of approximately 2,150 m, short of the Tioga-age shoreline of Glacial Lake Russell (Putnam, 1949), the larger, Pleistocene-age version of Mono Lake, which had a shoreline elevation of approximately 2,030 m during the inferred maximum extent of the Tioga glaciation about 20,500 years ago (Ali, 2018).

During the Tioga glaciation, a great ice field occupied the area in and around Tuolumne Meadows, with ice thicknesses exceeding 500 m. Only steep-sided and sharp-crested peaks and ridges, and a few wind-swept plateaus near the Sierra crest, projected above the ice. Peaks and ridges surrounded on all sides by ice are termed nunataks (an Eskimo term meaning "lonely peak"). Small nunataks in Yosemite National Park included Mount Conness, Cathedral Peak, Matthes Crest (fig. 1), and Snow Peak; larger nunataks included Clouds Rest and Rancheria Mountain north of Hetch Hetchy Valley. Nunataks act as refuge for species seeking to escape the advancing ice, and many former nunataks, like the plateau northeast of Mount Dana, now harbor rare or endemic plant species (see, for example, Rundel, 2011).

In addition to the major ice fields and valley glaciers in the Tuolumne and Merced River drainage basins, smaller, isolated glaciers existed on prominent peaks and ridges far to the west of the Sierra crest. These areas include the ridges south of Siesta Lake, small basins northwest of Buena Vista Peak, the slopes surrounding Mount Raymond, and the ridges north and east of Little Shuteye Peak. East of the Sierra crest, particularly in and around Lee Vining Canyon, a few small cirque glaciers were dominantly or entirely debris covered (see, for example, Clark and others, 1994). Debris likely accumulated on these glaciers because of abundant rockfalls (perhaps earthquake triggered) from fractured cirque headwalls, coupled with relatively slow rates of ice movement.

As the glaciers moved downslope through a combination of ice deformation and basal slip, they plucked and scoured the bedrock, leaving behind distinctive features such as tarns, streamlined bedforms, glacial polish, and striations. The vast quantities of eroded rock debris were transported to the lower ice margins, forming large lateral and terminal moraines; moraines are especially well preserved in the valleys and basins east of the Sierra crest.

As the climate warmed at the end of the Last Glacial Maximum, the Yosemite landscape deglaciated rapidly, with ice receding back to the highest cirques by approximately 15,000 years ago (Clark, 1976; Smith and Anderson, 1992; Guyton, 1998; James and others, 2002; Phillips and others, 2009; Phillips, 2016). The retreating ice left behind nested recessional moraines and large swaths of glacially polished bedrock dotted with erratic boulders (fig. 2). The Sierra Nevada was essentially deglaciated by 15,000 to 14,000 years ago (Clark and Gillespie, 1997), except for a brief readvance, termed the Recess Peak glaciation, which occurred at about 12,700 years ago (table 1; see also, Clark and Gillespie, 1997; Phillips, 2016). Glaciers associated with the Recess Peak advance extended only a few kilometers beyond the highest cirques.

Figure 1. Oblique aerial view to northeast, showing glacially carved peaks, spires, and arêtes in Cathedral Range south of Tuolumne Meadows in Yosemite National Park. Smooth, low-relief surfaces were covered by Tioga-age ice, whereas sharp, craggy peaks and ridges projected above ice surface. Prominent sunlit ridge in center-right of photograph is Matthes Crest, a glacial arête named in honor of François Matthes. Photograph by Josh Helling (used with permission).

Several small glaciers presently occupy north- and northeast-facing cirques in the Sierra Nevada (Guyton, 1998; Raub and others, 2006); in the map area, these include glaciers on the slopes of Mount Conness, Mount Dana, Mount Lyell, and Mount Maclure. These glaciers formed during or shortly before the Little Ice Age (Basagic and Fountain, 2011; Bowerman and Clark, 2011), a short cold period beginning about 600 years ago and ending about 150 years ago (Grove, 1988). In the Sierra Nevada, this glaciation is termed the Matthes advance (table 1; see also, Clark and Gillespie, 1997).

Tarns, which are lakes occupying bedrock depressions scoured out by glaciers (fig. 3), are prevalent in the Sierra Nevada and are a good indicator of the extent of Tioga-age ice (Moore and Moring, 2013). Tenaya Lake near Tuolumne Meadows is a prominent example. Other lakes within the Tioga-age ice extent are dammed by terminal or recessional moraines. Within the Yosemite map area, 87 percent of the 4,940 perennial lakes are located within the mapped extent of Tioga-age ice. Many of the 13 percent of lakes located outside of the Tioga-age ice extent are still related to that glaciation; for example, although Lukens Lake is located just outside of the Tioga-age ice extent, it is impounded by lateral moraines formed at that time.

In contrast to most lakes being situated within the Tioga-age ice extent, groves of Giant Sequoia (*Sequoiadendron giganteum*) on the western slope of the Sierra Nevada are located only outside of the Tioga-age ice extent (Moore and Mack, 2008). This is likely because glaciers scoured most of the soil from areas within the ice extent, leaving behind large expanses of bare granite or bouldery till deposits that are not amenable to Giant Sequoia growth (Muir, 1894).

Glaciation had a profound impact on the Yosemite landscape. In addition to sculpting most of the granite monoliths for which the park is famous, glaciation also dictated the distribution of many geological, hydrological, and ecological features. Thus, the lasting effects of Tioga glaciation are still readily observable in Yosemite National Park today.

Previous Work

The Yosemite region has been at the forefront of North American glacier research for more than 150 years (Guyton, 1998). Josiah D. Whitney, William H. Brewer, and Charles F. Hoffmann, of the newly created Geological Survey of California, were the first to document evidence of glaciation in the Sierra Nevada in the summer of 1863 as they were visiting the Tuolumne Meadows region:

Figure 2. Erratics, which are solitary boulders deposited by melting glaciers, resting on glacially polished and striated granitic bedrock along Murphy Creek, north of Tenaya Lake in Yosemite National Park.

> "[T]he whole region about the head of the Upper Tuolumne is one of the finest in the State for studying the traces of the ancient glacier system of the Sierra Nevada *** all of the phenomena of the moraines – lateral, medial, and terminal – are here displayed on the grandest scale" (Whitney, 1865, p. 428).

The following year, Whitney formed a survey party to explore the Sierra Nevada. The party included a young geologist named Clarence King, who would later go on to be the first director of the U.S. Geological Survey (USGS). King, an avid explorer and mountaineer, periodically struck out on his own, noting the various evidence for past glaciers in the landscape:

> "It was a two days' ramble all over the granite ridges, from the North Dome up to Lake Tenaya, during which I gathered ample evidence that a broad sheet of glacier, partly derived from Mount Hoffmann and in part from the Mount Watkins Ridge and Cathedral Peak, but mainly from the great Tuolumne glacier, gathered and flowed down into Yosemite Valley" (King, 1935).

Based on evidence in and around Yosemite Valley, King was the first to recognize that "a glacier no less than a thousand feet deep had flowed through the valley, occupying its entire bottom" (King, 1935).

The well-known naturalist John Muir first visited Yosemite in 1868, and the following year he spent the entire summer in Yosemite's high country, tracing the former passage of glaciers. By virtue of his extended studies, Muir developed a strong sense of the magnitude of glacial extent in Yosemite:

> "Already it is clear that all of the upper basins were filled with ice so deep and universal that but few of the highest crests and ridges were sufficiently great to separate it into individual glaciers, many of the highest mountains having been flowed over and rounded like the boulders in a river" (Muir, 1871).

Muir continued over many years to write enthusiastically about the evidence for glacier occupation and the profound role that glaciers played in sculpting Yosemite's landscapes (see, for example, Muir, 1880). Joseph LeConte, of the recently established University of California, first met Muir in Yosemite in 1870, and the two spent

Figure 3. Spiller Lake in Yosemite National Park, a tarn that occupies bedrock basin carved out by glacial erosion during Tioga glaciation.

time together in the Yosemite high country, observing glacial features. LeConte generally agreed with Muir's views, but he offered a somewhat more tempered perspective on the magnitude and extent of glacial erosion in the Sierra Nevada (LeConte, 1873). Shortly thereafter, USGS geologist Israel Russell investigated the paths that glaciers took from the crest of the Sierra Nevada eastward into Mono Basin, noting in the well-preserved moraines evidence for at least two distinct glaciations (Russell, 1889).

The first detailed map showing the ice extent in and around Yosemite Valley during the Tioga glaciation was published by USGS geologist François Matthes in his definitive "Geologic History of the Yosemite Valley" (Matthes, 1930). Matthes recognized evidence for three glacial periods, and he referred to the most recent one as the "Wisconsin" ("Wisconsin" is a general term for the most recent glacial period on the North American continent; in the Sierra Nevada, the Tahoe glaciation is correlated to the "early Wisconsin," and the Tioga glaciation is correlated with the "late Wisconsin"; Sharp and Birman, 1963). A topographer by training, Matthes took a map-based approach to his study of Yosemite's glaciers, identifying and correlating moraines across valleys, mapping trimlines on the peaks and ridges, and recording other glacial marginal features. Matthes later used similar techniques to map the "Wisconsin" ice extent in the upper San Joaquin River drainage basin along the south boundary of Yosemite National Park (Matthes, 1960) and farther south in Sequoia National Park (Matthes, 1965).

As Matthes conducted his mapping on the western slope of the Sierra Nevada, Stanford University geologist Elliot Blackwelder studied the better preserved glacial evidence east of the Sierra crest. He established the names and basic stratigraphic framework for four past glaciations, including the Tioga glaciation (table 1; see also, Blackwelder, 1931). Blackwelder (1931) described the primary features left behind by the Tioga glaciation:

> "The glacial features that were made by the ice tongues of the Tioga epoch are even now almost as fresh and unaltered as at the time of their formation *** Acres of polished and grooved rock are a familiar sight *** The lateral moraines generally stand out as bold embankments *** The terminal moraines are still complete, except for V-shaped notches through which the main streams tumble down to the plains beyond" (Blackwelder, 1931, p. 882).

Matthes and Blackwelder attempted to reconcile their sequences of multiple glaciations across the Sierra crest, but they were challenged by the lack of numerical age control, a challenge that continues to this day (Gillespie and Zehfuss, 2004).

Many researchers have subsequently investigated various aspects of glaciation in the map area. In creating this map, we integrated previously published information on glacial extent from 15-minute geologic quadrangle maps (Rinehart and others, 1964; Huber and Rinehart, 1965; Kistler, 1966, 1973; Huber, 1968, 1983; Bateman and others, 1971, 1983; Peck, 1980, 2002; Dodge and Calk, 1987; Bateman, 1989; Wahrhaftig, 2000), regional geologic maps (Bailey, 1989; Huber and others, 1989; Hildreth and Fierstein, 2016), and other publications that address Tioga-age ice extent and glacier flow directions in Yosemite National Park and vicinity (Matthes, 1930, 1960; Putnam, 1950; Birman, 1964; Clark, 1967, 1968; Curry, 1971; Sharp, 1972; Balogh, 1976, 1987; Gillespie, 1982; Phillips and others, 1990, 1996; Bursik and Gillespie, 1993; Clark and others, 2003; Gillespie and Clark, 2011; Rood and others, 2011). In general, we adopted this earlier work without major revisions, but there were some exceptions: for example, in the San Joaquin River drainage, we used Matthes' (1960) mapping of the "Wisconsin" ice extent and Birman's (1964) mapping of the Tahoe-age ice extent, but we inferred that they both represent the extent of Tioga-age ice, an interpretation supported by recent cosmogenic beryllium-10 (^{10}Be)-exposure dating of moraine boulders in the area (Becker and others, 2017).

Maps showing the general extent of Tioga-age ice in Yosemite were included in several Sierra Nevada–wide compilations, although these maps were necessarily of low resolution (see, for example, Wahrhaftig and Birman, 1965; Bateman and Wahrhaftig, 1966; Clark and others, 2003). The first comprehensive map of the Tioga-age ice extent throughout Yosemite was a hand-drawn map, coauthored by Clyde Wahrhaftig, showing an oblique view from the west (Alpha and others, 1987). The map presented here builds directly on that work, showing the Tioga-age ice extent in plan view, correcting errors in the ice extent and flow directions, and reporting the methods, data, and interpretations upon which the map is based.

Methods

As with the many earlier studies of glaciers in Yosemite, the development of this map was based primarily on mapping the evidence of glacier occupation on the landscape during the Tioga glaciation. This involved investigations on three main fronts:

1. Determining the spatial extent of glacier ice during the Tioga glaciation,
2. Understanding the spatial patterns of ice flow, and
3. Determining ice-surface elevations.

This combined information allowed for reconstruction of the full extent of Tioga-age ice, glacier flow patterns, ice-surface topography, and thicknesses of the various glaciers and ice fields.

Determining the Tioga-Age Ice Extent

We mapped the spatial extent of Tioga-age glaciers by identifying glacial moraines, trimlines, and other features indicative of glacier margins (see, for example, Andrews, 1982). We mapped these features in the field, as well as with various remote-sensing methods, primarily using aerial photographs but also lidar-based digital elevation models (DEMs) and shaded-relief maps. In locations where the relative ages of moraines were unclear (for example, uncertainty as to whether a mapped moraine was Tioga in age, or was instead from an earlier, larger glaciation), we dated these features using cosmogenic ^{10}Be-exposure dating.

Field Mapping

In the lower elevations of the map area, we identified the Tioga-age ice extent by mapping the position of features created by sediment deposition along the ice margins, primarily lateral and terminal moraines associated with valley glaciers. Lateral moraines are typically well preserved throughout the map area (fig. 4). Terminal moraines are well defined in the basins east of the range crest but are generally poorly defined on the western slope. This difference is most likely related to the greater stability of glacier terminus positions east of the crest, compared to unstable terminus positions west of the crest (Phillips, 2017). The difference in moraine size may also be related to aspects of moraine preservation. For example, glaciers on the western slope usually terminated within steep-walled canyons, which are highly erosive environments, whereas glaciers on the eastern slope commonly terminated in open basins more conducive to moraine preservation. The western slope also generally has a wetter and, thus, more erosive climate than the eastern slope, owing to the substantial rainshadow east of the Sierra crest. It is also possible that moraines along the east side of the range crest were larger to begin with, owing to the greater degree of bedrock fracturing along the eastern slope and, hence, a greater ability for glaciers to erode by plucking fractured rock, as well as a greater abundance of rockfalls onto glaciers from peaks, cirques, and canyon walls (Glazner and Stock, 2010).

We assessed the relative age of moraines in the field on the basis of morphology preservation and degree of weathering. Compared to older moraines, which lie outboard of Tioga-age moraines, Tioga-age moraines exhibit sharper crests, a higher boulder density, and fresher (as opposed to more weathered) boulders (Blackwelder, 1931; Birman, 1964; Burke and Birkeland, 1979). Hummocky topography and small closed depressions are also more common within areas bounded by Tioga-age moraine deposits.

We further identified ice margins by the change from commonly bare, ice-scoured bedrock surfaces in glaciated areas to commonly soil-mantled and forested surfaces in nonglaciated areas (fig. 5). Jointing, bedding, and other bedrock structures are usually sharply etched on glaciated surfaces, whereas deep weathering and soil development commonly obscure them on nonglaciated surfaces (see, for example, Benn and Evans, 2013).

At higher elevations in the map area where glaciers are primarily erosional in nature and deposition of moraines is limited, we used erosional features to identify the upper ice margins. At the uppermost elevations, ice margins are commonly characterized by

Figure 4. View to west along crest of right-lateral Tioga-age moraine west of Moraine Dome in Yosemite National Park. Moraine is composed of rock debris that ranges in size from silt to boulders.

Figure 5. View of upper Merced River canyon east of Yosemite Valley, as seen looking northeast from summit of Mount Starr King. Prominent right-lateral moraine in center of photograph, which slopes slightly left, marks height of Tioga-age glacier that flowed down Merced River canyon from right to left. Below this moraine, glacier scoured away soil and weathered bedrock, leaving behind sculpted, bare bedrock surfaces, in contrast to soil-mantled and vegetation-covered landscape above moraine. Sharp peaks and ridges on distant skyline projected above Tioga-age ice surface.

abrupt changes from downslope-directed couloirs and sharp craggy spurs above the ice surface to smooth, downvalley-directed, streamlined topography below the ice surface (fig. 6). Trimlines are sharp boundaries in a landscape, typically in the form of prominent breaks in slope, that mark the former ice position (see, for example, Benn and Evans, 2013). Areas above trimlines are typically weathered and covered in soil, whereas areas below trimlines are typically bare, fresh bedrock exhibiting signs of glacial erosion such as striations or polish. Trimlines are also marked in some settings by the abrupt termination of avalanche chutes (fig. 6) where ice and snow previously moved out onto the glacier surface (Matthes, 1965). In areas lacking clear trimlines or other topographic indicators, we used other glacier erosional features, such as tarns, striations, flutes, polish, and erratics, as general indicators of the presence of Tioga-age ice.

We interpreted isolated sharp-crested ridges and craggy, pointed peaks within the glaciated area as nunataks that were not overridden by ice. Rounded summits generally indicate that those summits were overridden by ice, with one major caveat: the domes surrounding Yosemite Valley and the Illilouette Creek basin (for example, North Dome, Half Dome, and Mount Starr King) were most likely never overtopped by ice; their rounded shape is because of exfoliation along sheeting joints (Huber, 1987; Glazner and Stock, 2010).

Remote-Sensing Mapping

Remote-sensing methods can be especially effective for mapping glacial geomorphology, as they can reveal features that are difficult to discern in the field (Hubbard and Glasser, 2005).

The initial mapping of ice extents, conducted in the 1980s, used aerial photographs as the primary remote-sensing data source (Allum, 1966). Subsequent to these initial efforts, the advent of DEMs, which digitally render topography in three dimensions, has significantly improved the resolution and accuracy of remote-sensing mapping. In particular, the advent of lidar-based topographic mapping has allowed for high-resolution (<1 m) topographic mapping. For mapping, lidar data are also advantageous because they can be filtered to remove vegetation, yielding "bare earth" models unlike those derived from conventional imagery such as aerial photographs. Differences in surface texture between glacially scoured bedrock and soil-mantled hillslopes are clearly resolved in these bare earth images. Additionally, many glacial landforms such as lateral and terminal moraines (fig. 7) are resolved in filtered lidar data in ways that are not possible using other remote-sensing methods (Smith and others, 2006).

We digitized the initial ice extents, overlaid them on lidar-based DEMs in ArcGIS, and viewed them in three dimensions, adjusting the ice margins so that they matched more precisely the glacier marginal features visible in the DEMs. We also used digital imagery derived from planes and satellites, most notably from the U.S. Department of Agriculture's National Agricultural Imagery Program, the USGS's Landsat program, and the European Space Agency's Copernicus program.

The ice extents were projected onto a 10-m-resolution DEM. Note that this DEM represents the modern topography and, therefore, shows some landforms, such as parts of the Mono Craters, that were not present during the Tioga glaciation.

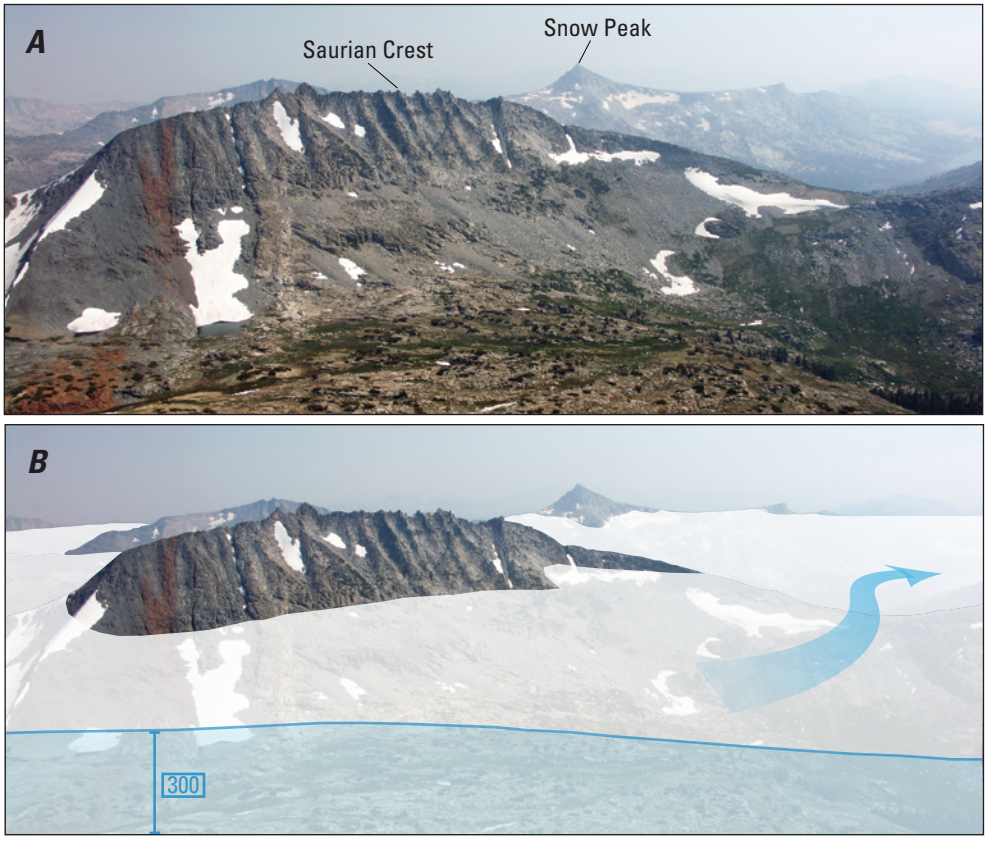

Figure 6. View to south from summit of Forsyth Peak, showing features mapped in field that were used to help determine Tioga-age ice extent in Yosemite National Park. Glacial arête of Saurian Crest is in foreground, and Snow Peak is in background. *A*, Transition between serrated arête crest and smoother ridges on either side provides approximate sense of height of past glaciers. Glacial trimline, identified by prominent break in slope and abrupt truncation of avalanche chutes, marks height of Tioga-age ice surface on north side of Saurian Crest. *B*, Same view as in *A*, with overlay showing approximate extent (transparent white shading) and direction of flow (blue arrow) of Tioga-age ice. Transparent blue shading in lower part of image shows approximate thickness of ice; height of trimline on Saurian Crest indicates glacier thickness of about 300 m, suggesting that ice completely surrounded it and flowed from northeast to southwest across pass to west.

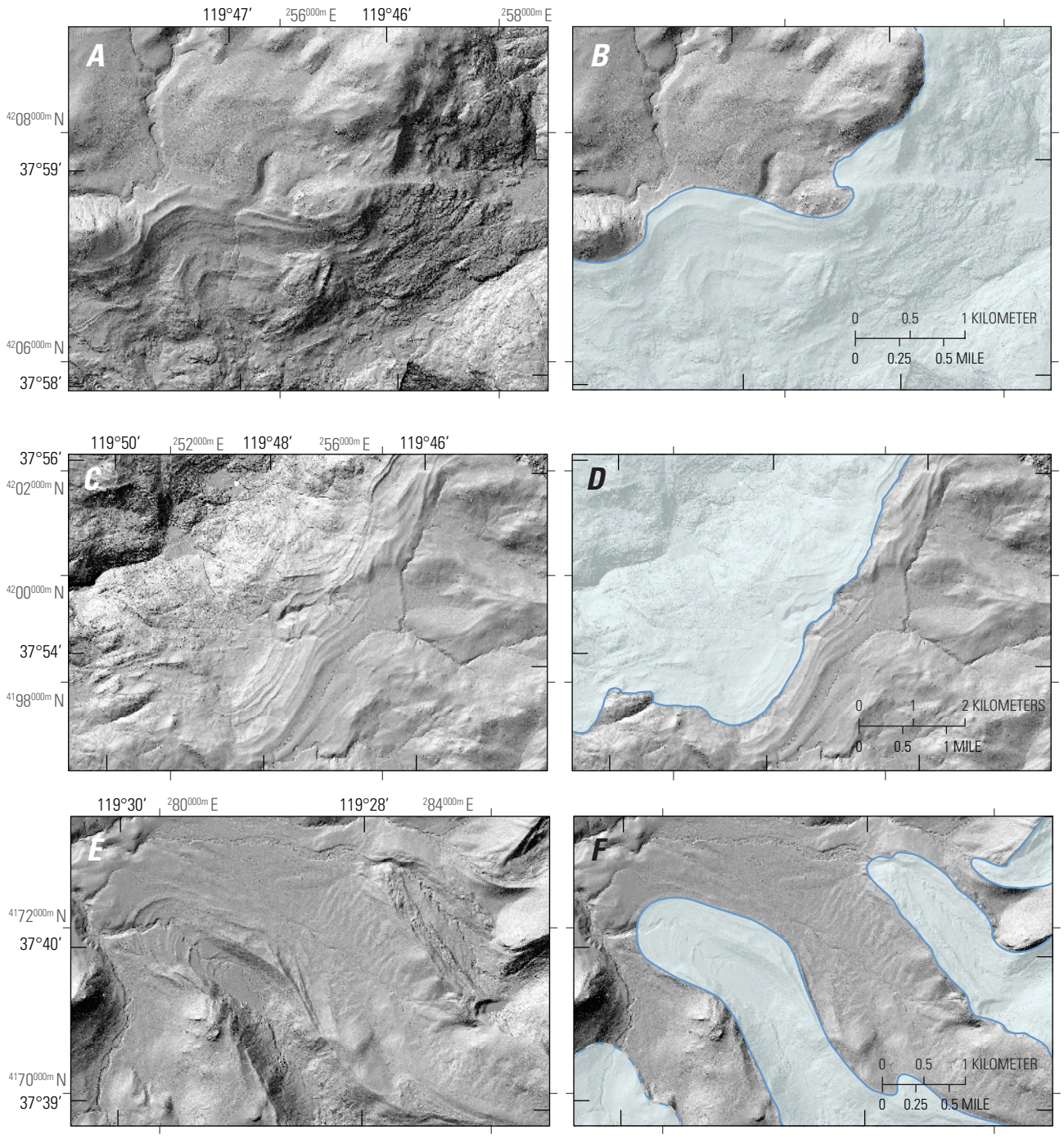

Figure 7. Shaded-relief maps showing examples of remotely sensed mapping of Tioga-age ice extent (pale-blue transparent overlays) in Yosemite National Park, using filtered ("bare earth") airborne-lidar data. Blue lines indicate limit of ice extent (dashed where approximately located). *A*, Map of north rim of Grand Canyon of the Tuolumne River north of Hetch Hetchy Valley, showing landscape differences between areas that were glaciated (lower right of *A*), which display rough texture of jointed, bare bedrock where soil has been scoured away, and areas that were not glaciated (upper left of *A*), which display smooth, weathered, soil-mantled surfaces. Several distinct lateral moraines delineate transition between these areas. *B*, Same area as *A*, showing mapped edge of Tioga-age glacier north of Hetch Hetchy Valley, based on features shown in *A*. *C*, Map of south rim of Grand Canyon of the Tuolumne River near Cottonwood Creek, showing landscape differences between areas that were glaciated (upper left of *C*) and areas that were not (lower right of *C*). Outermost lateral moraine, which retains relatively sharp crest, is inferred to represent maximum Tioga-age ice extent; more diffused moraines positioned outside of that are from older, larger glaciation, likely Tahoe-age advance. *D*, Same area as *C*, showing mapped edge of Tioga-age glacier near Cottonwood Creek, based on features shown in *C*. *E*, Map of upper Illilouette Creek area, showing terminal and recessional moraines and small closed depressions resulting from glaciers originating from Clark Range. *F*, Same area as *E*, showing mapped extent of Tioga-age ice in upper Illilouette Creek area, based on features shown in *E*.

Cosmogenic-Nuclide-Exposure Dating of Glacial Deposits

With the basic ice extent established, we evaluated marginal positions and ice thicknesses in certain areas by dating moraine boulders and erratics with cosmogenic-nuclide-exposure dating. Cosmogenic-nuclide-exposure dating of rock surfaces is based on the principle that cosmic-ray bombardment produces distinct nuclides that accumulate in rocks exposed near (that is, within ~1 m of) the Earth's surface at known rates (Gosse and Phillips, 2001). This dating technique is often applied to moraine boulders or glacial erratics (see, for example, Fabel and Harbor, 1999; Ivy-Ochs and others, 2007; Balco, 2011). The resulting ages indicate how long boulders have been exposed to cosmic rays and, by inference, how long ago those boulders were deposited by glaciers. Cosmogenic-nuclide-exposure dating has been used to date some Tioga-age moraines in the map area (Phillips and others, 1990, 1996; Rood and others, 2011) and elsewhere in the Sierra Nevada (James and others, 2002; Phillips and others, 2009; Pierce and others, 2017), generally yielding ages of more than 20,000 to about 17,000 years for the maximum ice extent (Phillips, 2016).

We employed cosmogenic-nuclide-exposure dating (specifically, using the nuclide ^{10}Be) in several ways to help determine the Tioga-age glacier extent. In some settings within the map area where adjacent parallel moraines exhibit similar weathering characteristics, it was difficult to distinguish between pre–Tioga-age moraines, Tioga-age maximum moraines, and Tioga-age recessional moraines. In these settings, we employed reconnaissance-level exposure dating of moraine boulders to help differentiate between moraines. We also used ^{10}Be-exposure dating to determine the age of erratics perched on domes and ridges, thereby ascertaining whether glacial ice had overtopped them during the Tioga glaciation. As these erratics would have been deposited during deglaciation, after the ice had reached its maximum extent and was in the process of retreating, they would record the time that dome surfaces became free of ice, rather than the timing of the maximum Tioga-age extent. In all, we collected 32 rock samples from 13 locations from moraine boulders and erratics in the lower elevation regions of the map area (fig. 8; see also, appendix 1).

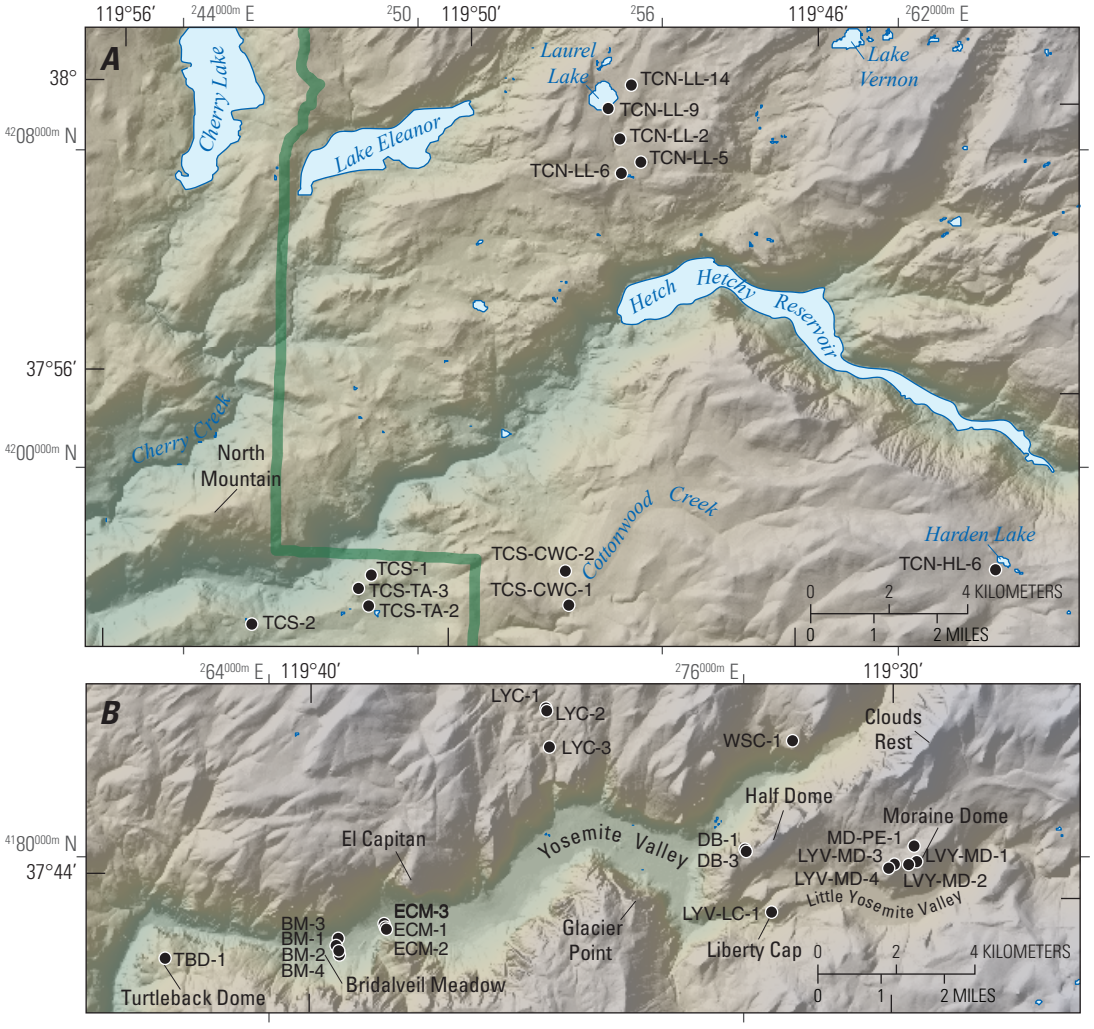

Figure 8. Maps showing sample localities (dots) for cosmogenic ^{10}Be-exposure dating of moraine boulders and glacial erratics in vicinity of (*A*) Grand Canyon of the Tuolumne River near Hetch Hetchy Valley, and (*B*) Yosemite Valley. ^{10}Be-exposure ages are reported in table 2; age data are provided in appendix 1. Green line shows boundary of Yosemite National Park.

Table 2. Mean cosmogenic ^{10}Be-exposure ages from inferred Tioga-age moraine boulders and erratics in Yosemite National Park.

[Age data provided in appendix 1]

Location	Feature type	Number of samples	Mean ^{10}Be-exposure age, in thousands of years
North of Hetch Hetchy Valley	Lateral moraine	1	25.4±3.2
Mather ("Camp Mather")	Lateral moraine	4	18.6±2.1
Cottonwood Creek	Lateral moraine	1	13.8±1.4
Lower part of Yosemite Creek	Terminal moraine	3	19.5±2.2
Bridalveil Moraine (just east of Bridalveil Meadow)	Terminal(?) moraine	4	16.5±2.1
El Capitan Moraine (at the base of El Capitan)	Recessional moraine	3	20.4±3.0
Liberty Cap	Erratic	1	17.4±1.7
Half Dome (Diving Board)	Lateral moraine	2	27.3±2.9
Mount Watkins (Snow Creek)	Lateral moraine	1	19.8±2.0
Moraine Dome	Lateral moraine, erratic	5	23.0±2.5

Cosmogenic ^{10}Be-exposure ages fall into two broad categories that clearly distinguish Tioga-age moraines from older moraines. Most of the inferred Tioga-age moraine boulders and erratics yield exposure ages of between approximately 23,000 and 16,000 years (table 2; see also, appendix 1), with an average age of approximately 19,000 years. This result is consistent with previous estimates of the timing of the various pulses of the Tioga glaciation in the Sierra Nevada (Phillips and others, 1996, 2009; Bischoff and Cummins, 2001; James and others, 2002; Phillips, 2016, 2017; Pierce and others, 2017), as well as with the timing of Last Glacial Maximum glaciations elsewhere in the western United States (see, for example, Gosse and others, 1995; Licciardi and Pierce, 2008; Leonard and others, 2017). However, there are several ^{10}Be-exposure-age outliers from Tioga-age deposits (appendix 1), indicating influences from either moraine degradation for the younger ages or predepositional inheritance for the older ages (Heyman and others, 2011).

In a few cases, the ^{10}Be-exposure ages provided compelling evidence for slightly adjusting the previously mapped ice extent, for example along the north rim of Hetch Hetchy Valley (fig. 8*A)*. In other cases, the ^{10}Be-exposure ages did not resolve existing uncertainty. For example, ^{10}Be-exposure ages from two glacially transported boulders on the west shoulder of Half Dome (fig. 8*B*; 19,290±1,990 and 35,220±3,850 years; see also, appendix 1) indicate that Tioga-age ice may have reached that high, but the discrepancy in ages is significant enough to reduce confidence in this result. Finally, there is at least one instance where a ^{10}Be-exposure age apparently conflicts with other evidence. The summit of Liberty Cap, south of Half Dome, was previously mapped as projecting above the Tioga-age ice extent (Alpha and others, 1987), on the basis of the height of lateral moraines in Little Yosemite Valley and the presence of summit weathering pans, which are generally not present on bedrock scoured during the Tioga glaciation (Birman, 1964; Huber, 1987). However, a polished, striated erratic boulder from the summit (fig. 7*B)* yielded a ^{10}Be-exposure age of 17,400±1,720 years (see appendix 1). This exposure age, clearly coinciding with the Last Glacial Maximum, suggests that Liberty Cap was indeed overtopped by ice during the Tioga glaciation, although probably only by thin ice and for only a short time period during the maximum ice extent.

Concentrations of ^{10}Be in moraine boulders and erratics from outside of the inferred Tioga-age ice extent indicate that these boulders are indeed considerably older than the Last Glacial Maximum (appendix 1). However, because of factors involving boulder erosion and nuclide decay, the dated pre–Tioga-age boulders do not provide reliable ^{10}Be-exposure ages for the older glaciations; rather, the majority of these boulders only record that they are substantially older than the Tioga glaciation (see appendix 1).

Determining Ice-Flow Directions

In addition to mapping the Tioga-age ice extent, we determined the directions that the major ice streams flowed. The direction of ice flow is dictated by the surface slope of the glacier (see, for example, Hooke, 2005; Benn and Evans, 2013; Cuffey and Paterson, 2010). As ice builds up at the higher elevations, it will begin to flow down the existing topography, generally following fluvially carved canyons. However, as large ice fields form, burying bedrock divides, the flow of ice will follow the overall surface slope of those ice fields, becoming less sensitive to the underlying topography. For example, the direction of ice flow across the basins and plateaus north of the Grand Canyon of the Tuolumne River was parallel to the ice flow in adjacent major canyons, rather than toward these canyons, because the entire area was covered by an ice field that had an overall slope toward the Grand Canyon of the Tuolumne River.

In general, glacier flow directions in and around Yosemite National Park were relatively simple, following the major drain-

ages of the Merced and Tuolumne Rivers. However, in several locations near the present-day drainage divides (for example, along the crest of the Sierra Nevada and the divide between the Merced and Tuolumne Rivers near Tuolumne Meadows), glacier flow directions were more complicated, in both space and time. We therefore focused our mapping efforts in these areas.

To determine general ice-flow directions, we identified subglacial bedforms that were streamlined by glacier flow. These include "lee-and-stoss" bedforms, which have an asymmetry developed through glacial erosion and (or) deposition that was recognizable in aerial photographs and filtered lidar data. We also inferred ice-flow directions from glacial striations, flutes, streamlined till deposits, and boulder trains of glacial erratics that had distinctive lithologies from particular rock outcrops.

Streamlined Bedforms

Streamlined bedforms sculpted by glaciers can indicate glacier flow directions (see, for example, Benn and Evans, 2013; Munro-Stasiuk and others, 2013). We mapped and measured the orientations of streamlined features in the field, from aerial photographs, and from filtered lidar data. Streamlined bedforms in the map area include asymmetrical roche moutonnées (fig. 9), bedrock outcrops having "crag-and-tail" morphologies, and both rock drumlins (also known as "whalebacks") and sediment drumlins. These features have a gradual slope facing toward the approaching ice and a steeper slope facing away from the approaching ice.

Erratics and Boulder Trains

Glacier flow directions can also be determined by tracing glacial erratics and moraine boulders that have distinctive lithologies back along a flow line to the bedrock outcrop where they originated. This technique is especially effective when the source lithology is unique and confined to a small area (fig. 10; see also, for example, Shilts, 1973; Syverson, 1995). In the northeastern part of the map area, in the vicinity of Snow Peak and Richardson Peak, boulder dispersal trains and field limits of glacial erratics from distinctive bedrock sources delineate specific glacier flow paths (fig. 11).

A large and persistent boulder train of metamorphic rocks derived from Mount Dana and the mountain immediately south of it (Mount Gibbs) extends from near the base of Mount Dana westward toward the Grand Canyon of the Tuolumne River, indicating westward ice flow through Tuolumne Meadows (fig. 12*B)*. Also in this area, glacial erratics of the Cathedral Peak Granodiorite are present near Tioga Pass (Huber, 2007; Glazner and Stock, 2010). These boulders must have come from bedrock exposures of the Cathedral Peak Granodiorite in the vicinity of Mount Conness (fig. 12*B*). Although the main glacier in upper Lee Vining Canyon turned eastward and flowed down Lee Vining Canyon into the Mono Basin, both the metamorphic boulder trains and the Cathedral Peak Granodiorite erratics indicate that, during the maximum extent of the Tioga glaciation, some ice flowed southward across Tioga Pass, joining other glaciers to form the Tuolumne icefield.

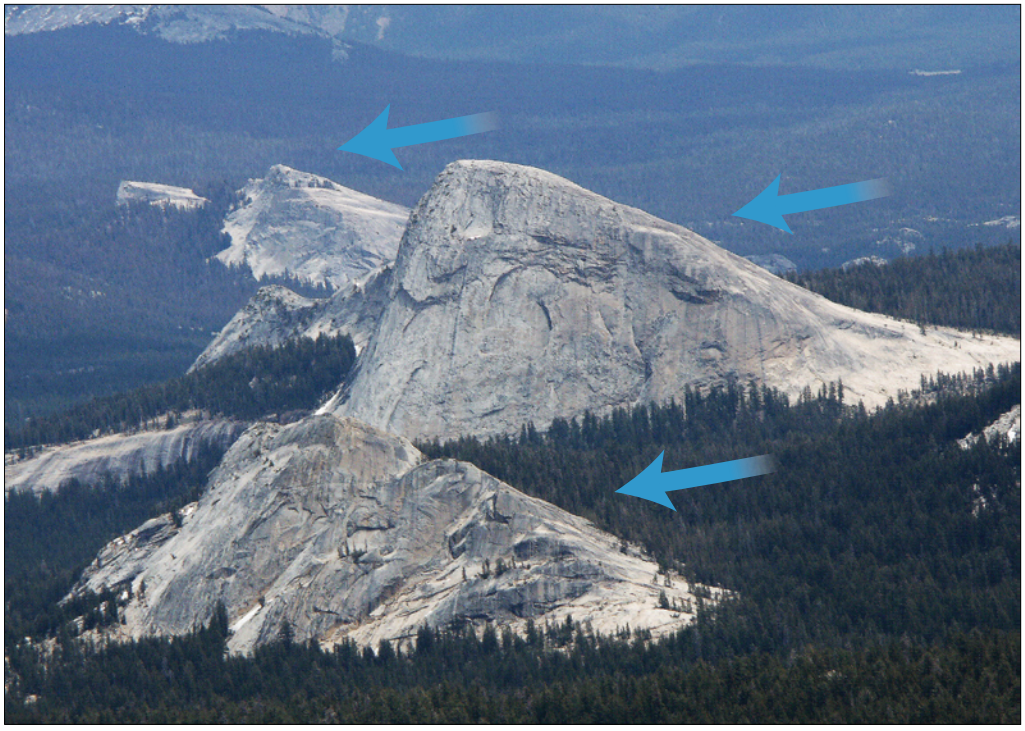

Figure 9. Roche moutonnées near Tuolumne Meadows in Yosemite National Park. Roche moutonnées are asymmetrical bedrock domes that have gentle stoss sides and steep lee sides. Glacial polish, striations, and erratics on Fairview Dome, tallest dome in center, demonstrate that all these domes were overtopped by ice during Tioga glaciation, a fact noted by John Muir: "The summit [of Fairview Dome] is burnished and scored *** the scratches and striae indicating that the mighty Tuolumne Glacier swept over it as if it were only a mere boulder in the bottom of the channel" (Muir, 1912). Overall asymmetrical shape of these bedforms, combined with striation orientations and other ice-flow indicators, show that direction of ice flow (blue arrows) was from right to left.

Glacial Striations and Other Bedrock Features

Glacial striations are linear scratches in bedrock that form underneath glaciers as rock fragments embedded in the ice are dragged across the bedrock during glacier sliding (fig. 13). As linear features, striations constrain the direction of glacier sliding to one of two directions (separated by 180°) (see, for example, Kleman, 1990; Hubbard and Glasser, 2005). In mountainous settings, it is usually straightforward to determine the sliding direction on the basis of the overall topographic setting. However, some interpretation is always required, and, in some settings (usually around passes and ridges overtopped by ice), it can be difficult to confirm the sliding direction (appendix 2). Additional directional indicators, such as lee-and-stoss bedforms, can help to identify sliding directions.

We measured mean orientations of glacial striations at nearly 700 sites (mean orientations derived from 3 to 5 individual measurements) throughout the map area (appendix 2). We also incorporated orientations from previous studies of striations and other directional indicators (Balogh, 1976, 1987). In general, striation orientations agree well with other flow indicators, although they may deviate locally in areas of complex bedrock topography.

At several sites, we measured two sets of crosscutting striations (appendix 2), which probably resulted from a change in the ice-flow direction as glaciers retreated. At Tioga Pass, for example, the clearest set of striations indicate a northeastward flow direction, away from Tioga Pass (fig. 12). However, a northeastward flow direction is in contrast to the southward ice-flow direction indicated by the presence of boulders of the Cathedral Peak Granodiorite, as discussed above. These apparently conflicting lines of evidence can be reconciled in a scenario in which the ice flowed southward across Tioga Pass during the maximum extent of the Tioga glaciation, then it reversed course as glaciers receded from that maximum position (fig. 12). In fact, another, subtle set of striations near Tioga Pass indicate southward ice flow; these striations presumably formed at the same time as the Cathedral Peak Granodiorite boulders were being deposited by southward flow over Tioga Pass, and then they were overprinted by a later set of striations pointing northeastward that formed as the ice receded and reversed course toward Lee Vining Canyon. This situation highlights a potential concern when using striations for inferring ice-flow directions during maximum glacial extents: because they are surficial features, striations can be readily overprinted or even erased by subsequent changes in flow directions during glacial recession. Striations may thus reflect only the most recent direction of ice movement, rather than the dominant direction during the maximum ice extent.

Determining Ice-Surface Elevations

We represented ice-surface elevations with contour lines connecting areas of equal elevation across the ice surface. At the ice margin, the elevation of the ice surface is the same as that of the landscape. Thus, we drew ice-surface contours by

Figure 10. Erratic of the dark-colored granodiorite of Kuna Crest resting on the lighter colored Cathedral Peak Granodiorite near summit of Lembert Dome, in Tuolumne Meadows in Yosemite National Park. This erratic was transported at least 7 km by Tioga-age glacier that flowed generally westward from near Sierra crest.

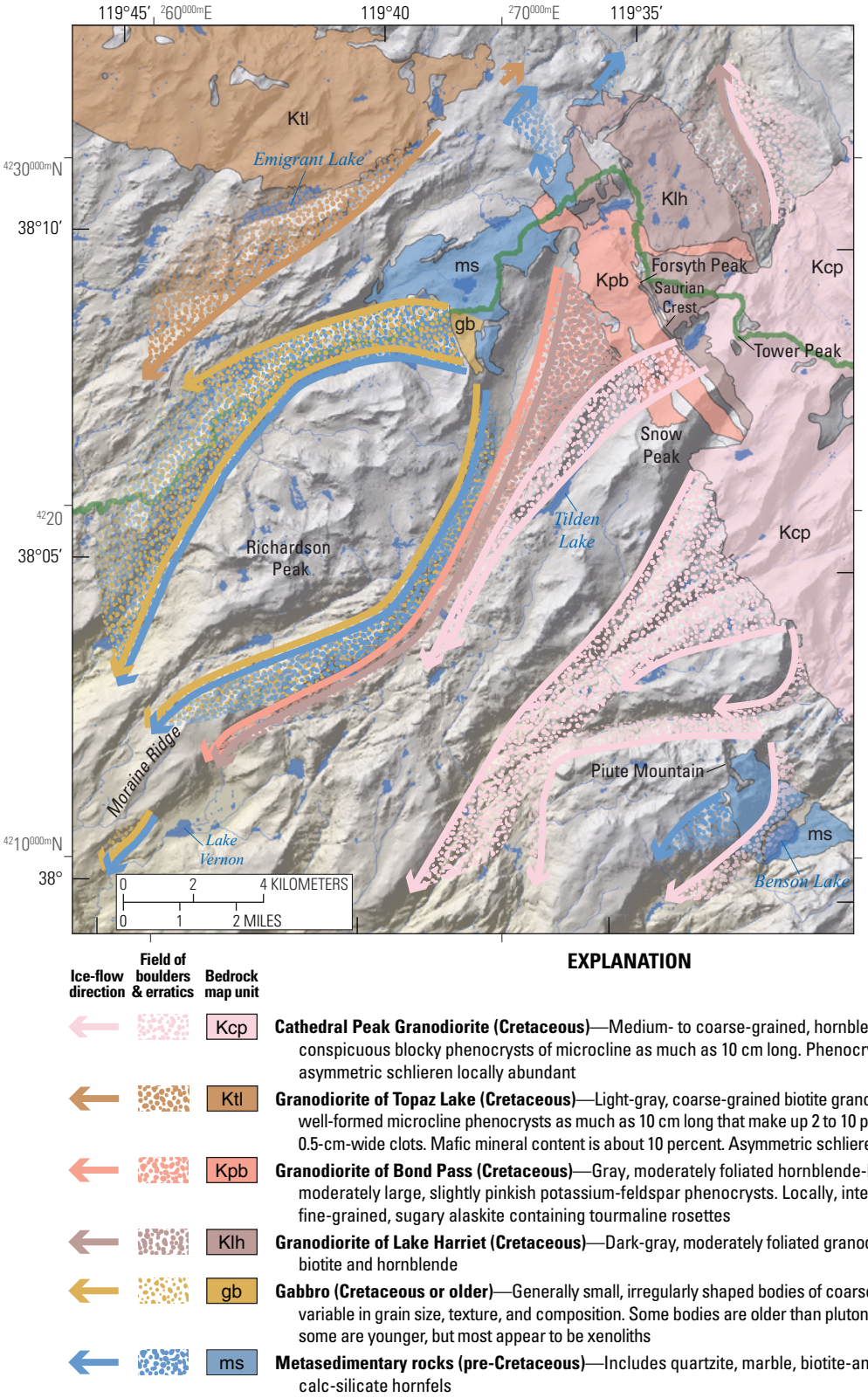

Figure 11. Shaded-relief map showing boulder-dispersal trains and fields of erratics (stippled areas) from certain bedrock map units in northeastern part of Yosemite National Park. Arrows, which show likely ice-flow directions indicated by distribution of boulder-dispersal trains, also delineate limits of erratic fields. Green line shows boundary of Yosemite National Park. Bedrock map units from Wahrhaftig (2000). Shaded-relief base map derived from 10-m digital elevation model from U.S. Geological Survey's National Elevation Dataset (available at https://ned.usgs.gov/).

connecting areas of equal elevation on either side of the ice margin, where the ice-surface elevation was well known. We then determined the slope of the glacier surface; as glacier flow direction is dictated not by the topography of the glacier bed but, instead, by the slope of the ice surface, the ice surface shown on the map must agree with the ice-flow patterns determined using the methods described in the previous section. Thus, over the surface of the glacier, we oriented the ice-surface contours perpendicular to the overall local ice-flow direction. Ice-surface contours are generally concave-up in the glacier accumulation areas, straight near the equilibrium line, and concave-down in the ablation areas (Benn and Evans, 2013).

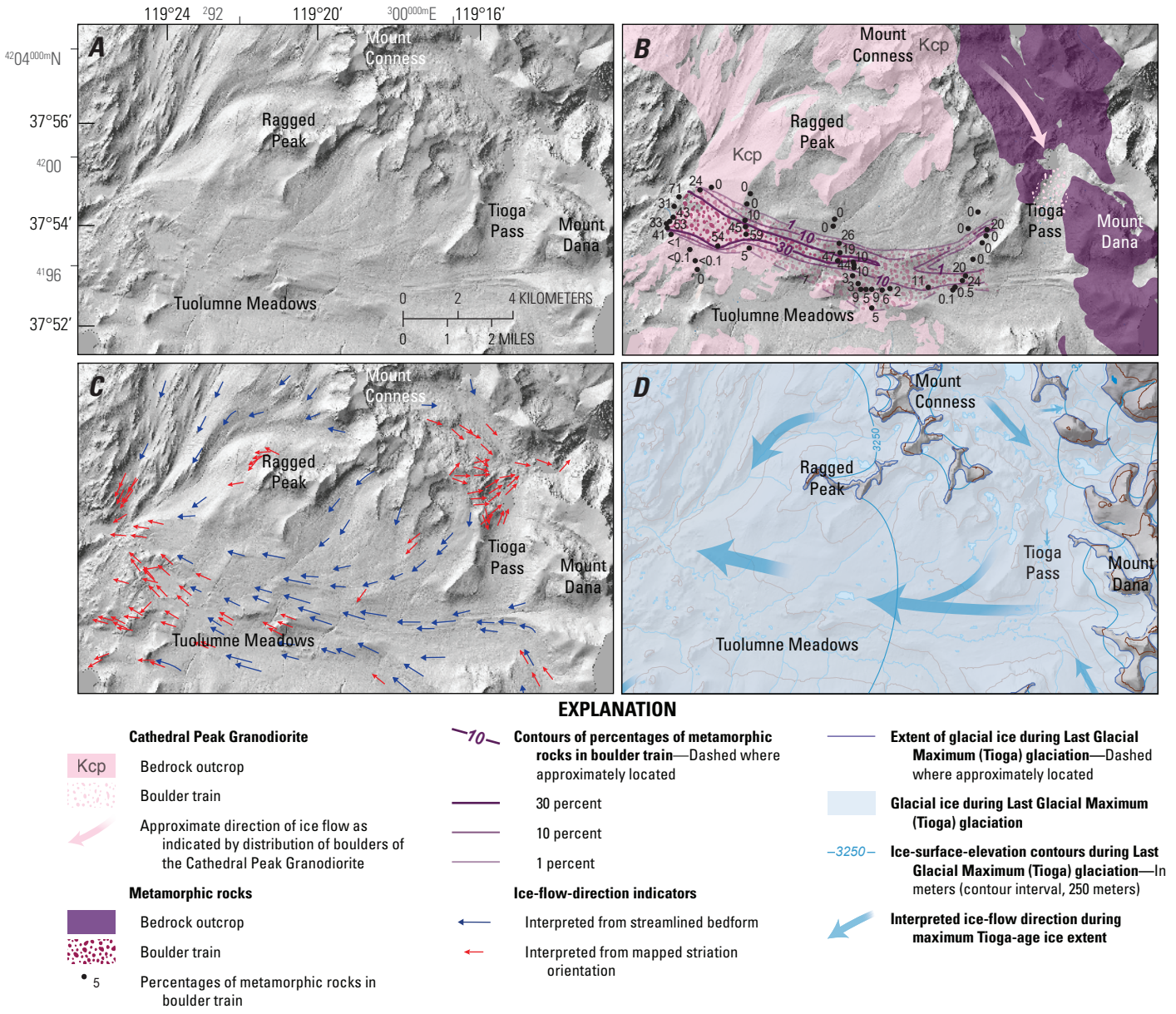

Figure 12. Shaded-relief maps of area around Tuolumne Meadows and Tioga Pass in Yosemite National Park, showing ice-flow directions determined from field and remote-sensing mapping. Shaded-relief base map derived from 1-m-resolution filtered airborne-lidar data. *A*, Map showing streamlined bedforms such as crag-and-tails and moraines. *B*, Same area as *A*, showing distribution of distinctive bedrock lithologies, as well as of glacial deposits composed of those lithologies, which reveal ice-flow directions. Erratics (boulders) of the Cathedral Peak Granodiorite at Tioga Pass originated from bedrock exposures near Mount Conness and were transported by ice flowing southward toward Tioga Pass (Huber, 2007). Large, persistent boulder train of metamorphic rocks north of Tuolumne Meadows was transported by ice flowing westward from metamorphic rocks near Mount Dana. Bedrock geology simplified from Huber and others (1989). *C*, Same area as *A*, showing mapped glacial striations and streamlined bedforms that indicate directions of basal ice flow. Striations near Tioga Pass indicate that ice flowed northeastward, away from Tioga Pass, opposite to flow direction inferred from boulders of the Cathedral Peak Granodiorite shown in *B*. These apparently conflicting lines of evidence can be reconciled using scenario in which ice flowed southward across Tioga Pass during time of maximum ice extent and then subsequently reversed course as glaciers receded. *D*, Same area as *A*, with overlay that shows ice extent and ice-flow directions during time of maximum ice extent.

Representing Uncertainty

In some locations, ambiguity in the field and in the remote-sensing data dictate that we infer ice extents and ice-surface contours, rather than map them definitively. We represent these features on the map with a dashed line.

The mapped ice extent in some areas is uncertain either because definitive evidence (for example, an obvious and well-dated terminal moraine) is lacking or because the existing evidence is conflicting or otherwise ambiguous. Whereas glacier-terminus positions on the east side of the Sierra crest typically extended out into basins and valleys, leaving depositional

landforms that remain well preserved, terminus positions on the west side of the crest typically were set within deep canyons, steep and highly erosive environments that prohibit the preservation of moraines and other glacial features. For example, in the vicinity of the inferred glacier-terminus position in the Grand Canyon of the Tuolumne River, there is only subtle evidence of glacial till and no clear terminal moraine; glacial striations approximately 1 km upcanyon of the inferred terminus position (see appendix 2) provide only a limiting constraint. Accordingly, we show the Tioga-age terminus position in the Grand Canyon of the Tuolumne River as a dashed line. The situation is similarly unclear for the terminus of the glacier that flowed down the San Joaquin River canyon southwest of Balloon Dome, which was set deep within a bedrock gorge (Matthes, 1960; Birman, 1964).

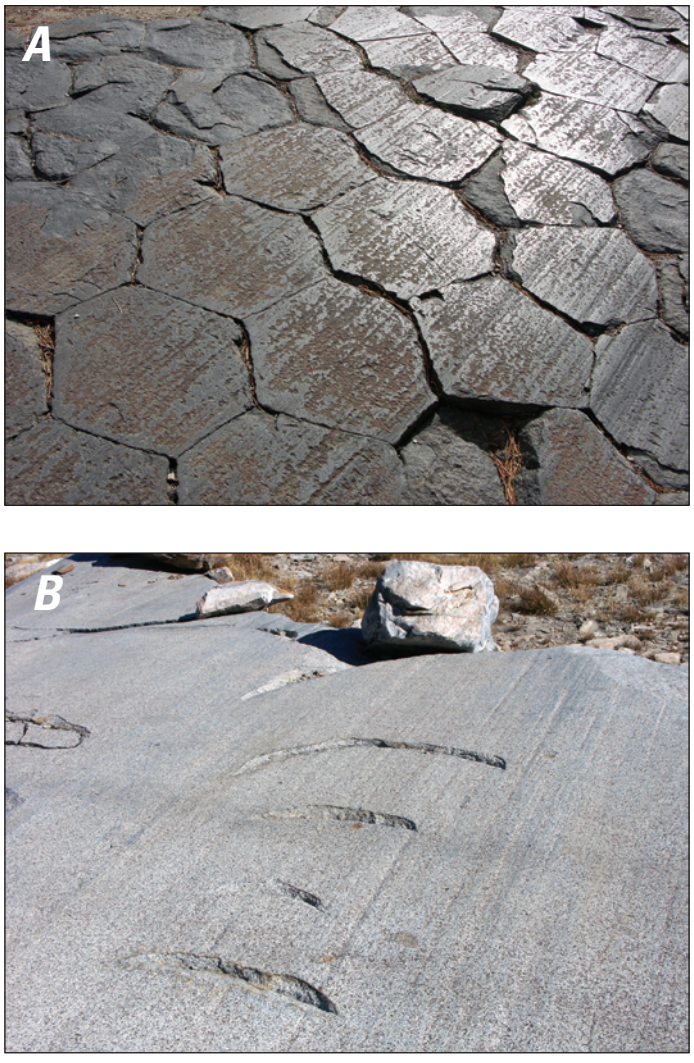

Figure 13. Glacial striations in Yosemite National Park. *A,* Striations on top of columnar-jointed basalt at Devils Postpile. *B,* Striations and crescentic gouges (also known as chattermarks) on granitic bedrock in upper Lyell Canyon. In both panels, sliding direction of ice was from lower left to upper right, along trend of glacial striations and, in *B*, perpendicular to crescentic gouges.

In Yosemite Valley, the inferred terminal moraine near Bridalveil Meadow (Huber, 1987) is relatively small and has likely been modified by the Merced River; ^{10}Be-exposure ages from boulders on this moraine show a high degree of scatter (appendix 1) and do not allow for discriminating between a terminal moraine deposited during the maximum glacier extent and a recessional moraine deposited after deglaciation had already begun. Furthermore, because of the steep cliffs in Yosemite Valley, lateral moraines are not preserved, nor is there a well-defined trimline. For these reasons, the ice extent throughout most of Yosemite Valley is also dashed. We note the possibility that the actual terminus position of the glacier in Yosemite Valley may have extended a few kilometers farther down the canyon than shown. Finally, we must infer the ice extent north of Mammoth Mountain because Holocene volcanism from the Inyo and Mono Craters (Bailey, 1989; Hildreth and Fierstein, 2016) buried most of the glacial deposits in that area under tephra, prohibiting delineation of glacial extent on the basis of moraines.

Ice-surface elevations are also uncertain in some areas. For example, we could not reliably determine ice elevations and ice-surface contours at the ice dome northeast of Forsyth Peak because of a lack of adjacent elevation markers such as trimlines on adjacent ridges or nunataks. Ice-surface contours are also dashed on the glacier north of Mammoth Mountain because of the lack of moraine preservation there. Finally, wherever ice extents are approximate, ice-surface-elevation contours in these areas are also approximate and, therefore, shown as dashed.

References Cited

Ali, G., 2018, Late glacial and deglacial fluctuations of Mono Lake, California: New York, Columbia University, Ph.D. dissertation, 227 p., https://doi.org/10.7916/D8CC2BNN.

Allum, J.A.E., 1966, Photogeology and regional mapping: Oxford, Pergamon Press, 107 p.

Alpha, T.R., Wahrhaftig, C., and Huber, N.K., 1987, Oblique map showing maximum extent of 20,000-year-old (Tioga) glaciers, Yosemite National Park, central Sierra Nevada, California: U.S. Geological Survey Miscellaneous Investigations Series Map I–1885, https://pubs.usgs.gov/imap/i1885/.

Andrews, J.T., 1982, On the reconstruction of Pleistocene ice sheets—A review: Quaternary Science Reviews, v. 1, no. 1, p. 1–30, https://doi.org/10.1016/0277-3791(82)90017-8.

Bailey, R.A., 1989, Geologic map of the Long Valley Caldera, Mono-Inyo Craters volcanic chain, and vicinity, eastern California: U.S. Geological Survey Miscellaneous Investigations Series Map I–1933, scale 1:62,500, https://pubs.er.usgs.gov/publication/i1933.

Balco, G., 2011, Contributions and unrealized potential contributions of cosmogenic-nuclide exposure dating to glacier chronology, 1990-2010: Quaternary Science Reviews, v. 30, nos. 1–2, p. 3–27, https://doi.org/10.1016/j.quascirev.2010.11.003.

Balogh, R.S., 1976, Subglacial fluvial erosion in the vicinity of Tuolumne Meadows, Yosemite National Park, California: Los Angeles, University of California, Ph.D. dissertation, 61 p.

Balogh, R.S., 1987, Pothole Dome—Where water flowed uphill—Tuolumne County: California Geology, v. 40, no. 7, p. 154–157.
Basagic, H.J., and Fountain, A.G., 2011, Quantifying 20th century glacier change in the Sierra Nevada, California: Arctic, Antarctic, and Alpine Research, v. 43, no. 3, p. 317–330, https://doi.org/10.1657/1938-4246-43.3.317.
Bateman, P.C., 1989, Geologic map of the Bass Lake quadrangle, west-central Sierra Nevada, California: U.S. Geological Survey Geologic Quadrangle Map GQ–1656, scale 1:62,500, https://pubs.er.usgs.gov/publication/gq1656.
Bateman, P.C., Kistler, R.W., Peck, D.L., and Busacca, A., 1983, Geologic map of the Tuolumne Meadows quadrangle, Yosemite National Park, California: U.S. Geological Survey Geologic Quadrangle Map GQ–1570, scale 1:62,500, https://pubs.er.usgs.gov/publication/gq1570.
Bateman, P.C., Lockwood, J.P., and Lydon, P.A., 1971, Geologic map of the Kaiser Peak quadrangle, central Sierra Nevada, California: U.S. Geological Survey Geologic Quadrangle Map GQ–894, scale 1:62,500, https://pubs.er.usgs.gov/publication/gq894.
Bateman, P.C., and Wahrhaftig, C., 1966, Geology of the Sierra Nevada, *in* Bailey, E.H., ed., Geology of northern California: California Division of Mines and Geology Bulletin 190, p. 105–172.
Becker, R.A., Barth, A.M., Marcott, S.A., and Tikoff, B., 2017, Constraining the timing and magnitude of deglaciation in the drainage basins of Mono Creek and the South Fork of the San Joaquin River, central Sierra Nevada mountains (USA): Geological Society of America, Abstracts with Programs, v. 49, no. 6, https://doi.org/10.1130/abs/2017AM-304611.
Benn, D.I., and Evans, D.J.A., 2013, Glaciers and glaciation (2d ed.): New York, Routledge, 802 p.
Benson, L.V., May, H.M., Antweiler, R.C., Brinton, T.I., Kashgarian, M., Smoot, J.P., and Lund, S.P., 1998, Continuous lake-sediment records of glaciation in the Sierra Nevada between 52,600 and 12,500 ^{14}C yr B.P.: Quaternary Research, v. 50, no. 2, p. 113–127, https://doi.org/10.1006/qres.1998.1993.
Birkeland, P.W., Burke, R.M, and Walker, A.L., 1980, Soils and subsurface rock-weathering features of Sherwin and pre-Sherwin glacial deposits, eastern Sierra Nevada, California: Geological Society of America Bulletin, v. 91, no. 4, p. 238–244, https://doi.org/10.1130/0016-7606(1980)91<238:SASRFO>2.0.CO;2.
Birman, J.H., 1964, Glacial geology across the crest of the Sierra Nevada, California: Geological Society of America Special Paper 75, 80 p.
Bischoff, J.L., and Cummins, K., 2001, Wisconsin glaciation of the Sierra Nevada (79,000–15,000 yr B.P.) as recorded by rock flour in sediment of Owens Lake, California: Quaternary Research, v. 55, no. 1, p. 14–24, https://doi.org/10.1006/qres.2000.2183.
Blackwelder, E., 1931, Pleistocene glaciation in the Sierra Nevada and the Basin Ranges: Geological Society of America Bulletin, v. 42, no. 4, p. 865–922, https://doi.org/10.1130/GSAB-42-865.
Bowerman, N.D., and Clark, D.H., 2011, Holocene glaciation of the central Sierra Nevada, California: Quaternary Science Reviews, v. 30, nos. 9–10, p. 1067–1085, https://doi.org/10.1016/j.quascirev.2010.10.014.
Burke, R.M., and Birkeland, P.W., 1979, Reevaluation of multiparameter relative dating techniques and their application to the glacial sequence along the eastern escarpment of the Sierra Nevada, California: Quaternary Research, v. 11, no. 1, p. 21–51, https://doi.org/10.1016/0033-5894(79)90068-1.
Bursik, M.I., and Gillespie, A.R., 1993, Late Pleistocene glaciation of Mono Basin, California: Quaternary Research, v. 39, no. 1, p. 24–35, https://doi.org/10.1006/qres.1993.1003.
Calkins, F.C, Huber, N.K., and Roller, J.A., 1985, Bedrock geologic map of Yosemite Valley, Yosemite National Park, California: U.S. Geological Survey Miscellaneous Investigations Series Map I–1639, 7 p., scale 1:24,000, https://pubs.er.usgs.gov/publication/i1639.
Clark, D.H., Clark, M.M., and Gillespie, A.R., 1994, Debris-covered glaciers in the Sierra Nevada, California, and their implications for snowline reconstructions: Quaternary Research, v. 41, no. 2, p. 139–153, https://doi.org/10.1006/qres.1994.1016.
Clark, D.H., and Gillespie, A.R., 1997, Timing and significance of late-glacial and Holocene cirque glaciation in the Sierra Nevada, California: Quaternary International, v. 38–39, p. 21–38, https://doi.org/10.1016/S1040-6182(96)00024-9.
Clark, D.H., Gillespie, A.R., Clark, M., and Burke, R., 2003, Mountain glaciations of the Sierra Nevada, *in* Easterbrook, D.J., ed., Quaternary geology of the United States: Reno, Nev., Desert Research Institute, INQUA 2003 Field Guide Volume, p. 287–311.
Clark, M.M., 1967, Pleistocene glaciation of the drainage of the West Walker River, Sierra Nevada, California: Palo Alto, Calif., Stanford University, Ph.D. dissertation, 130 p.
Clark, M.M., 1968, Pleistocene glaciation of the upper West Walker drainage, Sierra Nevada, California: Geological Society of America Special Paper 115, 317 p.
Clark, M.M., 1976, Evidence for rapid destruction of latest Pleistocene glaciers of the Sierra Nevada, California: Geological Society of America, Abstracts with Programs, v. 8, no. 3. p. 361–362.
Clark, P.U., Dyke, A.S., Shakun, J.D., Carlson, A.E., Clark, J., Wohlfarth, B., Mitrovica, J.X., Hostetler, S.W., and McCabe, A.M., 2009, The Last Glacial Maximum: Science, v. 325, no. 5941, p. 710–714, https://doi.org/10.1126/science.1172873.
Cuffey, K.M., and Paterson, W.S.B., 2010, The physics of glaciers (4th ed.): Burlington, Mass., Butterworth-Heinemann, 693 p.
Curry, R.R., 1971, Glacial and Pleistocene history of the Mammoth Lakes Sierra—A geologic guidebook: Missoula, University of Montana, Department of Geology Geological Series Publication No. 11, 49 p.
Dalrymple, G.B., 1963, Potassium-argon dates of some Cenozoic volcanic rocks of the Sierra Nevada, California: Geological Society of America Bulletin, v.

74, no. 4, p. 379–390, https://doi.org/10.1130/0016-7606(1963)74[379:PDOSCV]2.0.CO;2.
Dalrymple, G.B., 1964, Cenozoic chronology of the Sierra Nevada, California: University of California Publications in Geological Science, v. 45, 41 p.
Dodge, F.C.W., and Calk, L.C., 1987, Geologic map of the Lake Eleanor quadrangle, central Sierra Nevada, California: U.S. Geological Survey Geologic Quadrangle Map GQ–1639, scale 1:62,500, https://pubs.er.usgs.gov/publication/gq1639.
Fabel, D., and Harbor, J., 1999, The use of in-situ produced cosmogenic radionuclides in glaciology and glacial geomorphology: Annals of Glaciology, v. 28, p. 103–110, https://doi.org/10.3189/172756499781821968.
Fullerton, D.S., 1986, Chronology and correlation of glacial deposits in the Sierra Nevada, California: Quaternary Science Reviews, v. 5, p. 161–169, https://doi.org/10.1016/0277-3791(86)90181-2.
Gibbons, A.B., Megeath, J.D., and Pierce, K.L., 1984, Probability of moraine survival in a succession of glacial advances: Geology, v. 12, no. 6, p. 327–330, https://doi.org/10.1130/0091-7613(1984)12<327:POMSIA>2.0.CO;2.
Gillespie, A.R., 1982, Quaternary glaciation and tectonism in the southeastern Sierra Nevada, Inyo County, California: Pasadena, California Institute of Technology, Ph.D. dissertation, 695 p.
Gillespie, A.R., and Clark, D.H., 2011, Glaciations of the Sierra Nevada, California, USA, *in* Ehlers, J., Gibbard, P.L., and Hughes, P.D., eds., Quaternary glaciations - Extent and chronology—A closer look: Developments in Quaternary Science, v. 15, p. 447–462, https://doi.org/10.1016/B978-0-444-53447-7.00034-9.
Gillespie, A.R., and Zehfuss, P.H., 2004, Glaciations of the Sierra Nevada, California, USA, *in* Ehlers, J., and Gibbard, P.L., eds., Quaternary glaciations - Extent and chronology, Part II—North America: Developments in Quaternary Science, v. 2, pt. B, p. 51–62, https://doi.org/10.1016/S1571-0866(04)80185-4.
Glazner, A.F., and Stock, G.M., 2010, Geology underfoot in Yosemite National Park: Missoula, Mont., Mountain Press, 300 p.
Gosse, J.C., Klein, J., Lawn, B., Middleton, R., and Evenson, E.B., 1995, Beryllium-10 dating of the duration and retreat of the last Pinedale glacial sequence: Science, v. 268, no. 5215, p. 1329–1333, https://doi.org/10.1126/science.268.5215.1329.
Gosse, J.C., and Phillips, F.M., 2001, Terrestrial in situ cosmogenic nuclides—Theory and application: Quaternary Science Reviews, v. 20, no. 14, p. 1475–1560, https://doi.org/10.1016/S0277-3791(00)00171-2.
Grove, J.M., 1988, The Little Ice Age: London, Methuen, 498 p.
Guyton, B., 1998, Glaciers of California: Berkeley, Calif., University of California Press, 197 p.
Heyman, J., Stroeven, A.P., Harbor, J.M., and Caffee, M.W., 2011, Too young or too old—Evaluating cosmogenic exposure dating based on an analysis of compiled of boulder exposure ages: Earth and Planetary Science Letters, v. 302, nos. 1–2, p. 71–80, https://doi.org/10.1016/j.epsl.2010.11.040.
Hildreth, W., and Fierstein, J., 2016, Eruptive history of Mammoth Mountain and its mafic periphery, California: U.S. Geological Survey Professional Paper 1812, 128 p., 2 plates, scale 1:24,000, https://doi.org/10.3133/pp1812.
Hooke, R.L., 2005, Principles of glacier mechanics: Cambridge, Cambridge University Press, 429 p.
Hubbard, B., and Glasser, N., 2005, Field techniques in glaciology and glacial geomorphology: Hoboken, N.J., John Wiley & Sons Inc., 400 p.
Huber, N.K., 1968, Geologic map of the Shuteye Peak quadrangle, Sierra Nevada, California: U.S. Geological Survey Geologic Quadrangle Map GQ–728, scale 1:62,500, https://pubs.er.usgs.gov/publication/gq728.
Huber, N.K., 1981, Amount of timing of late Cenozoic uplift and tilt of the central Sierra Nevada, California—Evidence from the upper San Joaquin River basin: U.S. Geological Survey Professional Paper 1197, 28 p., https://pubs.er.usgs.gov/publication/pp1197.
Huber, N.K., 1983, Preliminary geologic map of the Pinecrest quadrangle, central Sierra Nevada, California: U.S. Geological Survey Miscellaneous Field Studies Map MF–1437, scale 1:62,500, https://pubs.er.usgs.gov/publication/mf1437.
Huber, N.K., 1987, The geologic story of Yosemite National Park: U.S. Geological Survey Bulletin 1595, 64 p., https://pubs.er.usgs.gov/publication/b1595.
Huber, N.K., 2007, Geological ramblings in Yosemite: Berkeley, Calif., Heyday, 121 p.
Huber, N.K., Bateman, P.C., and Wahrhaftig, C., 1989, Geologic map of Yosemite National Park and vicinity: U.S. Geological Survey Miscellaneous Investigations Series Map I–1874, scale 1:125,000, https://pubs.usgs.gov/imap/i1874/.
Huber, N.K., and Rinehart, C.D., 1965, Geologic map of the Devils Postpile quadrangle, Sierra Nevada, California: U.S. Geological Survey Geologic Quadrangle Map GQ–437, scale 1:62,500, https://pubs.er.usgs.gov/publication/gq437.
Ivy-Ochs, S., Kerschner, H., and Schlüchter, C., 2007, Cosmogenic nuclides and the dating of Lateglacial and Early Holocene glacier variations—The Alpine perspective: Quaternary International, v. 164–165, p. 53–63, https://doi.org/10.1016/j.quaint.2006.12.008.
James, L.A., Harbor, J., Fabel, D., Dahms, D., and Elmore, D., 2002, Late Pleistocene glaciations in the northwestern Sierra Nevada, California: Quaternary Research, v. 57, no. 3, p. 409–419, https://doi.org/10.1006/qres.2002.2335.
Kessler, M.A., Anderson, R.S., and Stock, G.M., 2006, Modeling topographic and climatic control of east-west asymmetry in Sierra Nevada glacier length during the Last Glacial Maximum: Journal of Geophysical Research—Earth Surface, v. 111, no. F2, https://doi.org/10.1029/2005JF000365.
King, C., 1935 (1872), Mountaineering in the Sierra Nevada, ed. F.P. Farquhar: W.W. Norton & Co., New York, 320 p.
Kistler, R.W., 1966, Geologic map of the Mono Craters quadrangle, Mono and Tuolumne Counties, California: U.S. Geological Survey Geologic Quadrangle Map GQ–462, scale 1:62,500, https://pubs.er.usgs.gov/publication/gq462.

Kistler, R.W., 1973, Geologic map of the Hetch Hetchy Reservoir quadrangle, Yosemite National Park, California: U.S. Geological Survey Geologic Quadrangle Map GQ–1112, scale 1:62,500, https://pubs.er.usgs.gov/publication/gq1112.

Kleman, J., 1990, On the use of glacial striae for reconstruction of palaeo-ice sheet flow patterns: Geografiska Annaler, v. 72, nos. 3–4, p. 217–236, https://doi.org/10.1080/04353676.1990.11880318.

LeConte, J., 1873, On some of the ancient glaciers of the Sierra: American Journal of Science and Arts, v. 5, no. 29, p. 325–339.

Leonard, E.M., Laabs, B.J.C., Plummer, M.A., Kroner, R.K., Brugger, K.A., Spiess, V.M., Refsnider, K.A., Xia, Y., and Caffee, M.W., 2017, Late Pleistocene glaciation and deglaciation in the Crestone Peaks area, Colorado Sangre de Cristo Mountains, USA—Chronology and paleoclimate: Quaternary Science Reviews, v. 158, p. 127–144, https://doi.org/10.1016/j.quascirev.2016.11.024.

Licciardi, J.M., and Pierce, K.L., 2008, Cosmogenic exposure-age chronologies of Pinedale and Bull Lake glaciations in greater Yellowstone and the Teton Range, USA: Quaternary Science Reviews, v. 27, nos. 7–8, p. 814–831, https://doi.org/10.1016/j.quascirev.2007.12.005.

Matthes, F.E., 1929, Multiple glaciation in the Sierra Nevada: Science, v. 70, no. 1803, p. 75–76, https://doi.org/10.1126/science.70.1803.75.

Matthes, F.E., 1930, Geologic history of the Yosemite Valley: U.S. Geological Survey Professional Paper 160, 137 p., https://pubs.er.usgs.gov/publication/pp160.

Matthes, F.E., 1950, The incomparable valley—A geologic interpretation of the Yosemite: Berkeley, Calif., University of California Press, 160 p.

Matthes, F.E., 1960, Reconnaissance of the geomorphology and glacial geology of the San Joaquin Basin, Sierra Nevada, California: U.S. Geological Survey Professional Paper 329, 62 p., https://pubs.er.usgs.gov/publication/pp329.

Matthes, F.E., 1965, Glacial reconnaissance of Sequoia National Park, California: U.S. Geological Survey Professional Paper 504–A, 56 p., 2 plates, scale 1:125,000, https://pubs.er.usgs.gov/publication/pp504A.

Moore, J.G., and Mack, G.S., 2008, Map showing limits of Tahoe Glaciation in Sequoia and Kings Canyon National Parks, California: U.S. Geological Survey Scientific Investigations Map 2945, scale 1:125,000, https://pubs.usgs.gov/sim/2945/.

Moore, J.G., and Moring, B.C., 2013, Rangewide glaciation in the Sierra Nevada, California: Geosphere, v. 9, no. 6, p. 1804–1818, https://doi.org/10.1130/GES00891.1.

Munro-Stasiuk, M.J., Heyman, J., and Harbor, J., 2013, Erosional features, *in* Giardino, J.R., and Harbor, J.M., eds., Treatise of geomorphology: Cambridge, Mass., Academic Press, p. 84–99.

Muir, J., 1871, Yosemite glaciers: New York Tribune, December 5, 1871.

Muir, J., 1880, The ancient glaciers of the Sierra: Californian, v. 2, no. 12, p. 550–557.

Muir, J., 1894, The mountains of California: New York, The Century Publishing Company.

Muir, J., 1912, The Yosemite: New York, The Century Publishing Company.

Nishiizumi, K., Winterer, E.L., Kohl, C.P., Klein, J., Middleton, R., Lal, D., and Arnold, J.R., 1989, Cosmic ray production rates of ^{10}Be and ^{26}Al in quartz from glacially polished rocks: Journal of Geophysical Research—Solid Earth, v. 94, no. B12, p. 17,907–17,915, https://doi.org/10.1029/JB094iB12p17907.

Peck, D.L., 1980, Geologic map of the Merced Peak quadrangle, central Sierra Nevada, California: U.S. Geological Survey Geologic Quadrangle Map GQ–1531, scale 1:62,500, https://pubs.er.usgs.gov/publication/gq1531.

Peck, D.L., 2002, Geologic map of the Yosemite quadrangle, central Sierra Nevada, California: U.S. Geological Survey Geologic Investigations Series Map I–2751, scale 1:62,500, https://pubs.er.usgs.gov/publication/i2751.

Phillips, F.M., 2016, Cosmogenic nuclide data sets from the Sierra Nevada, California, for assessment of nuclide production models—I. Late Pleistocene glacial chronology: Quaternary Geochronology, v. 35, p. 119–129, https://doi.org/10.1016/j.quageo.2015.12.003.

Phillips, F.M., 2017, Glacial chronology of the Sierra Nevada, California, from the Last Glacial Maximum to the Holocene: Cuadernos de Investigación Geográfica, v. 43, no. 2, p. 527–552, https://doi.org/10.18172/cig.3233.

Phillips, F.M., Zreda, M., Plummer, M.A., Elmore, D., and Clark, D.H., 2009, Glacial geology and chronology of Bishop Creek and vicinity, eastern Sierra Nevada, California: Geological Society of America Bulletin, v. 121, nos. 7–8, p. 1013–1033, https://doi.org/10.1130/B26271.1.

Phillips, F.M., Zreda, M.G., Benson, L.V., Plummer, M.A., Elmore, D., and Sharma, P., 1996, Chronology for fluctuations in late Pleistocene Sierra Nevada glaciers and lakes: Science, v. 274, no. 5288, p. 749–761, https://doi.org/10.1126/science.274.5288.749.

Phillips, F.M., Zreda, M.G., Smith, S.S., Elmore, D., Kubik, P.W., and Sharma, P., 1990, Cosmogenic chlorine-36 chronology for glacial deposits at Bloody Canyon, eastern Sierra Nevada: Science, v. 248, no. 4962, p. 1529–1532, https://doi.org/10.1126/science.248.4962.1529.

Pierce, K.D., Wesnousky, S.G., and Owen, L.A., 2017, Terrestrial cosmogenic surface exposure dating of moraines at Lake Tahoe in the Sierra Nevada of California and slip rate estimate for the West Tahoe Fault: Geomorphology, v. 298, p. 63–71, https://doi.org/10.1016/j.geomorph.2017.09.030.

Putnam, W.C., 1949, Quaternary geology of the June Lake district, California: Geological Society of America Bulletin, v. 60, no. 8, p. 1281–1302, https://doi.org/10.1130/0016-7606(1949)60[1281:QGOTJL]2.0.CO;2.

Putnam, W.C., 1950, Moraine and shoreline relationships at Mono Lake, California: Geological Society of America Bulletin, v. 61, no. 2, p. 115–122, https://doi.org/10.1130/0016-7606(1950)61[115:MASRAM]2.0.CO;2.

Raub, W., Brown, C.S., and Post, A., 2006, Inventory of glaciers in the Sierra Nevada, California: U.S. Geological Survey

Open-File Report 2006–1239, 228 p., 4 plates, https://pubs.usgs.gov/of/2006/1239/.

Rinehart, C.D., Ross, D.C., and Pakiser, L.C., 1964, Geology and mineral deposits of the Mount Morrison quadrangle, Sierra Nevada, California: U.S. Geological Survey Professional Paper 385, 106 p., 7 plates, https://pubs.er.usgs.gov/publication/pp385.

Rood, D.H., Burbank, D.W., and Finkel, R.C., 2011, Chronology of glaciations in the Sierra Nevada, California, from ^{10}Be surface exposure dating: Quaternary Science Reviews, v. 30, nos. 5–6, p. 646–661, https://doi.org/10.1016/j.quascirev.2010.12.001.

Rundel, P.W., 2011, The diversity and biogeography of the alpine flora of the Sierra Nevada, California: Madroño, v. 58, no. 3, p. 153–184, https://doi.org/10.3120/0024-9637-58.3.153.

Russell, I.C., 1889, Quaternary history of the Mono Valley, California: U.S. Geological Survey Eighth Annual Report, p. 267–394.

Sharp, R.P., 1968, Sherwin Till–Bishop Tuff geological relationships, Sierra Nevada, California: Geological Society of America Bulletin, v. 79, no. 3, p. 351–364, https://doi.org/10.1130/0016-7606(1968)79[351:STTGRS]2.0.CO;2.

Sharp, R.P., 1972, Pleistocene glaciation, Bridgeport Basin: Geological Society of America Bulletin, v. 83, no. 8, p. 2233–2260, https://doi.org/10.1130/0016-7606(1972)83[2233:PGBBC]2.0.CO;2.

Sharp, R.P., and Birman, J.H., 1963, Additions to classical sequence of Pleistocene glaciations, Sierra Nevada, California: Geological Society of America Bulletin, v. 74, no. 8, p. 1079–1086, https://doi.org/10.1130/0016-7606(1963)74[1079:ATCSOP]2.0.CO;2.

Shilts, W.W., 1973, Glacial dispersal of rocks, minerals, and trace elements in Wisconsin till, southeastern Quebec, Canada, *in* Black, R.F., Goldthwait, R.P., and Willman, H.B., eds., The Wisconsin Stage: Geological Society of America Memoir, v. 136, p. 189–219, https://doi.org/10.1130/MEM136-p189.

Smith, M.J., Rose, J., and Booth, S., 2006, Geomorphological mapping of glacial landforms from remotely sensed data—An evaluation of the principal data sources and an assessment of their quality: Geomorphology, v. 76, nos. 1–2, p. 148–165, https://doi.org/10.1016/j.geomorph.2005.11.001.

Smith, S.J., and Anderson, R.S., 1992, Late Wisconsin paleoecologic record from Swamp Lake, Yosemite National Park, California: Quaternary Research, v. 38, no. 1, p. 91–102, https://doi.org/10.1016/0033-5894(92)90032-E.

Stine, S., 1994, Extreme and persistent drought in California and Patagonia during mediaeval time: Nature, v. 369, p. 546–549, https://doi.org/10.1038/369546a0.

Syverson, K.M., 1995, The ability of ice-flow indicators to record complex, historic deglaciation events, Burroughs Glacier, Alaska: Boreas, v. 24, no. 3, p. 232–244, https://doi.org/10.1111/j.1502-3885.1995.tb00776.x.

Wahrhaftig, C., 2000, Geologic map of the Tower Peak quadrangle, central Sierra Nevada, California: U.S. Geological Survey Geologic Investigations Series I–2697, scale 1:62,500, https://pubs.usgs.gov/imap/i2697/.

Wahrhaftig, C., and Birman, J.H., 1965, The Quaternary of the Pacific mountain system in California, *in* Wright, H.E., Jr., and Frey, D.G., eds., The Quaternary of the United States: Princeton, N.J., Princeton University Press, p. 299–340.

Whitney, J.D., 1865, The High Sierra, chapter X *of* Geology—Volume I—Report of progress, and synopsis of field work from 1860 to 1864: Philadelphia, Pa., Caxton Press of Sherman & Co.

Wood, S.H., 1977, Distribution, correlation, and radiocarbon dating of late Holocene tephra, Mono and Inyo Craters, eastern California: Geological Society of America Bulletin, v. 88, no. 1, p. 89–95, https://doi.org/10.1130/0016-7606(1977)88<89:DCARDO>2.0.CO;2.

Glossary

ablation Loss of glacier ice by the combined processes of melting, evaporation, and calving.

arête A narrow, serrate mountain ridge that separates—or once separated—two adjacent glaciers.

boulder train A series or "train" of boulders, usually of distinctive lithology, deposited by a glacier; indicates glacier flow parallel to the series of boulders.

chattermark Arcuate fractures caused by glacial erosion of bedrock surfaces; these features are usually concave in the downflow direction and are oriented perpendicular to ice movement. Also called crescentic gouges.

cirque A deep, steep-walled, flat-floored, semicircular topographic basin created by glacial excavation high in mountainous areas, usually at the heads of valleys.

cosmogenic-nuclide-exposure dating A geologic dating method that measures the amount of time a particular deposit, for example, a glacial erratic, has been resting at Earth's surface, being exposed to cosmic rays.

couloir A narrow, deep gully or gorge on a mountainside.

crag-and-tail A streamlined hill or ridge, resulting from glaciation and consisting of a knob of resistant bedrock (the "crag"), with an elongate body (the "tail") of more erodible bedrock, till, or both, deposited on its lee side.

debris-covered glacier A glacier that is partly or wholly covered by debris, usually in its lower sections.

drumlin A low, smoothly rounded, elongate hill of compact glacial till or, rarely, other kinds of drift, either built under the margin of the ice and shaped by its flow or carved out of an older moraine by readvancing ice; its longer axis is parallel to the direction of movement of the ice. It usually has a blunt nose pointing in the direction from which the ice approached and a gentler slope tapering in the other direction. See also, "Rock drumlin."

end moraine A ridgelike accumulation of till that marks a stillstand position of a present or past glacier front.

equilibrium line altitude The elevation on a glacier surface where the annual mass balance is zero (in other words, where accumulation of snow is exactly balanced by ablation over a period of a year).

erratic A rock fragment carried by glacial ice and deposited at some distance from the outcrop from which it was derived, generally resting on bedrock of different lithology.

exfoliation The shedding of relatively thin layers of rock by the formation of joints that parallel the rock surface, typically resulting in a rounded rock mass or dome-shaped hill.

firn Wetted snow that survives the summer without being transformed into ice.

glacial striation One of multiple scratches or minute lines, generally parallel, inscribed on a rock surface by rock fragments embedded within a glacier.

glacier A large mass of ice formed on land by the compaction and recrystallization of snow, creeping downslope or outward owing to the stress of its own weight and surviving from year to year.

hanging valley A tributary valley with a floor that is distinctly higher than the main valley it joins; commonly this offset is due to differential erosion by glaciers of different sizes.

Holocene An epoch of the Quaternary Period, beginning about 11,700 years ago and lasting until the present.

ice field A very large, thick sheet of glacial ice generally flowing outward in at least two directions.

Last Glacial Maximum Timing of the largest extent and volume of ice on Earth during the last Ice Age, usually referring to the period between 26,000 and 18,000 years ago.

lateral moraine An accumulation of glacial till along the side margins of the lower parts of a glacier. The accumulations remain as ridges or embankments after the glacier has retreated.

lidar (light detection and ranging) A surveying method that uses pulsed laser light to measure distances, such as the distance

from a laser scanner to the ground surface. Lidar data may be collected from the air or from the ground, and they can be filtered to remove vegetation.

Little Ice Age A relatively brief cold period, lasting from approximately 1300 to 1850 C.E., when mountain glaciers expanded in both the Northern and Southern Hemispheres.

moraine A mound, ridge, or other distinct accumulation of unsorted, unstratified glacial drift, chiefly till, deposited by direct action of glacier ice.

nunatak An isolated hill, knob, ridge, or peak of bedrock that projects prominently above the surface of a glacier and is completely surrounded by glacier ice. Eskimo for "lonely peak."

Pleistocene An epoch of the Quaternary Period, beginning 2.6 million years ago and lasting until about 11,700 years ago; spans the Earth's most recent period of repeated glaciations.

Quaternary A period of the Cenozoic Era, beginning 2.6 million years ago and lasting until the present.

rainshadow An area having relatively little precipitation because of the effect of a topographic barrier, especially a mountain range, that causes the prevailing winds to lose their moisture on the windward side, causing the leeward side to be dry.

recessional moraine An end or lateral moraine built during a temporary but significant pause in the final retreat of a glacier. Also, a moraine built during a slight or minor readvance of the ice front during a period of general recession.

roche moutonnée A glacially sculptured knob of bedrock, with an upstream (stoss) side that is gently inclined, rounded, and striated, and a downstream (lee) side that is steep, rough, and hackly.

rock drumlin A hill having the form of a drumlin but consisting of bedrock, sometimes veneered with till. Also known as a "whaleback."

rock glacier A slow-moving accumulation of angular rock debris with interstitial ice or an ice core.

striation See glacial striation.

tarn A small glacial lake dammed by a lip of bedrock.

temperate glacier A glacier characteristic of the temperate zone, where the ice and firn that the glacier consists of are at the melting point, except for a thin surface layer that seasonally freezes.

tephra Airborne rock fragments produced by a volcanic eruption.

terminal moraine The outermost end moraine of a glacier or ice sheet, marking the maximum advance of the ice.

till Unstratified, unsorted rock debris, deposited directly by a glacier, without reworking by meltwater, and consisting of a mixture of clay, silt, sand, gravel, and boulders ranging widely in size and shape.

Tioga glaciation A glacial advance in the Sierra Nevada that occurred during the Last Glacial Maximum approximately 21,000 to 17,000 years ago.

trimline A boundary line delimiting the maximum upper level of the margins of a glacier that has receded from an area. It commonly separates jagged cliffs above from glacially smoothed rock surfaces below.

weathering pan Bedrock depressions formed where water collects in small natural pits and then enlarges these pits by weathering processes. Also known as solution pans.

Appendix 1. Sampling Considerations and Analytical Results of Cosmogenic Beryllium-10 (^{10}Be)-Exposure Dating of Moraine Boulders and Erratics in Yosemite National Park

Sampling Considerations

We collected granitic rock samples from the tops of moraine boulders and glacial erratics for cosmogenic beryllium-10 (^{10}Be)-exposure dating (fig. 1.1). We collected 32 samples from 13 locations in the lower elevations of the map area (table 1.1). Sample locations are shown in figure 8.

We carefully selected boulders in the field to minimize or avoid factors that can confound cosmogenic-nuclide-exposure ages, including (1) loss of nuclides by erosion of the boulder surface, (2) reduction of nuclide production in the boulder surface when it is covered by sediment or snow, and (3) inheritance of nuclides if the boulder was exposed to cosmic rays prior to deposition. All factors except for inheritance result in calculated exposure ages that are younger than the true exposure age.

In order to constrain the erosion rate of sampled boulder surfaces and, thus, to correct for (1) above, we measured ^{10}Be concentrations from three glacially transported boulders located well outside of the mapped Tioga-age ice extent. One boulder is located at Turtleback Dome, on the southwest rim of Yosemite Valley, and the other two are located between Laurel Lake and the north rim of the Grand Canyon of the Tuolumne River near Hetch Hetchy Valley (table 1.1; see also, fig. 8). All three areas are thought to have been glaciated well before the Tioga glaciation (Matthes, 1930; Putnam and others, 2013). Over long time scales, accumulation of cosmogenic ^{10}Be in a boulder surface reaches a state of secular equilibrium (commonly referred to as "saturation"), in which accumulation of cosmogenic nuclides equals loss of nuclides through radioactive decay and boulder erosion. Assuming steady-state boulder erosion, the ^{10}Be concentration therefore becomes a measure of the long-term erosion rate of the sampled surface (Lal, 1991). The three boulders from the pre–Tioga-age areas were saturated with respect to ^{10}Be, and they yielded a mean boulder-erosion rate of 0.00065 centimeters per year (cm/yr) (table 1.1). This rate is broadly similar to erosion rates of bare granitic bedrock surfaces measured with cosmogenic ^{10}Be elsewhere in the Sierra Nevada (0.0003–0.0010 cm/yr; Small and others, 1997; Stock and others, 2005). We therefore used an erosion rate of 0.00065 cm/yr for calculating exposure ages for the remaining boulders.

Rapid boulder erosion, especially spallation of rock slabs caused by wildfires, is a potentially significant factor affecting cosmogenic-nuclide-exposure ages because spallation can remove some, or all, of the accumulated ^{10}Be, leading to anomalously young exposure ages (see, for example, Bierman and Gillespie, 1991). However, our observations in recently burned areas suggest that the tops of boulders are mostly unaffected by spallation, and so we minimized the likelihood of sampling spalled surfaces by only sampling the tops of the tallest available boulders.

Degradation of moraine morphology has also been shown to have a potentially significant effect on cosmogenic-nuclide-exposure ages for moraine boulders (see, for example, Hallet and Putkonen, 1994; Putkonen and Swanson, 2003; Putkonen and

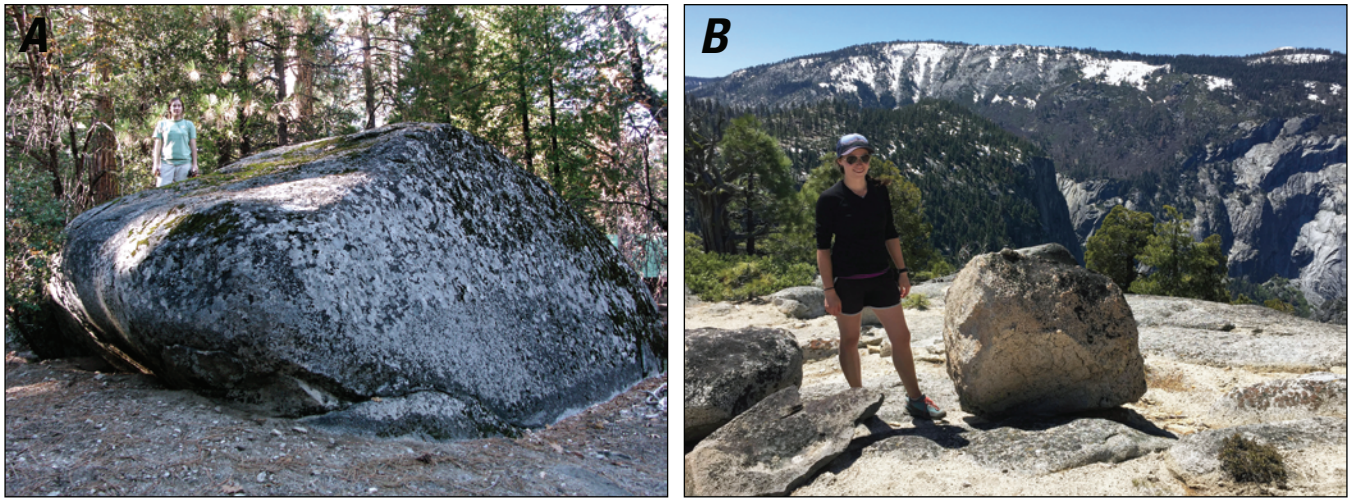

Figure 1.1. Examples of moraine boulders and glacial erratics sampled for cosmogenic ^{10}Be-exposure dating. *A*, Boulder (sample TCS-TA-3) on crest of left-lateral moraine near Mather (at "Camp Mather"), which yielded ^{10}Be-exposure age of 17,740±1,930 years, coinciding with Last Glacial Maximum (Tioga) glaciation. *B*, Glacial erratic (sample LYV-LC-1) on summit of Liberty Cap, which yielded ^{10}Be-exposure age of 17,400±1,720 years, indicating that summit of Liberty Cap was overtopped by ice during Tioga glaciation.

O'Neal, 2006; Applegate and others, 2010). In essence, as boulders previously buried within the moraine at the time of moraine deposition are slowly exhumed, they are progressively exposed; their exposure age is therefore younger than the depositional age of the moraine. We employed sampling strategies to avoid complications associated with moraine erosion, such as sampling the tops of numerous tall boulders situated on moraine crests (Putkonen and Swanson, 2003); the tops of tall boulders most likely projected above the original moraine surface prior to diffusion, and boulders on moraine crests have not rolled over. Concentrations of large, round boulders along the margins of moraines are an indication that boulder rolling may have occurred. Tall boulders also tend to project above the snow, reducing the effects of snow shielding on cosmogenic-nuclide production rates (Gosse and Phillips, 2001; Heyman and others, 2016).

Sample Analysis

Samples were chemically isolated for ^{10}Be following standardized methods (Kohl and Nishiizumi, 1992). ^{10}Be/^{9}Be ratios were determined by accelerator mass spectrometry at the Center for Accelerator Mass Spectrometry (CAMS) at the Lawrence Livermore National Laboratory, as well as at the Purdue Rare Isotope Measurement (PRIME) Laboratory.

Analytical Results

We calculated ^{10}Be-exposure ages for moraine boulders and erratics using the Cosmic-Ray Produced Nuclide Systematics (CRONUS) age calculator (Balco and others, 2008). Data are reported in table 1.1, and they are shown graphically in figure 1.2.

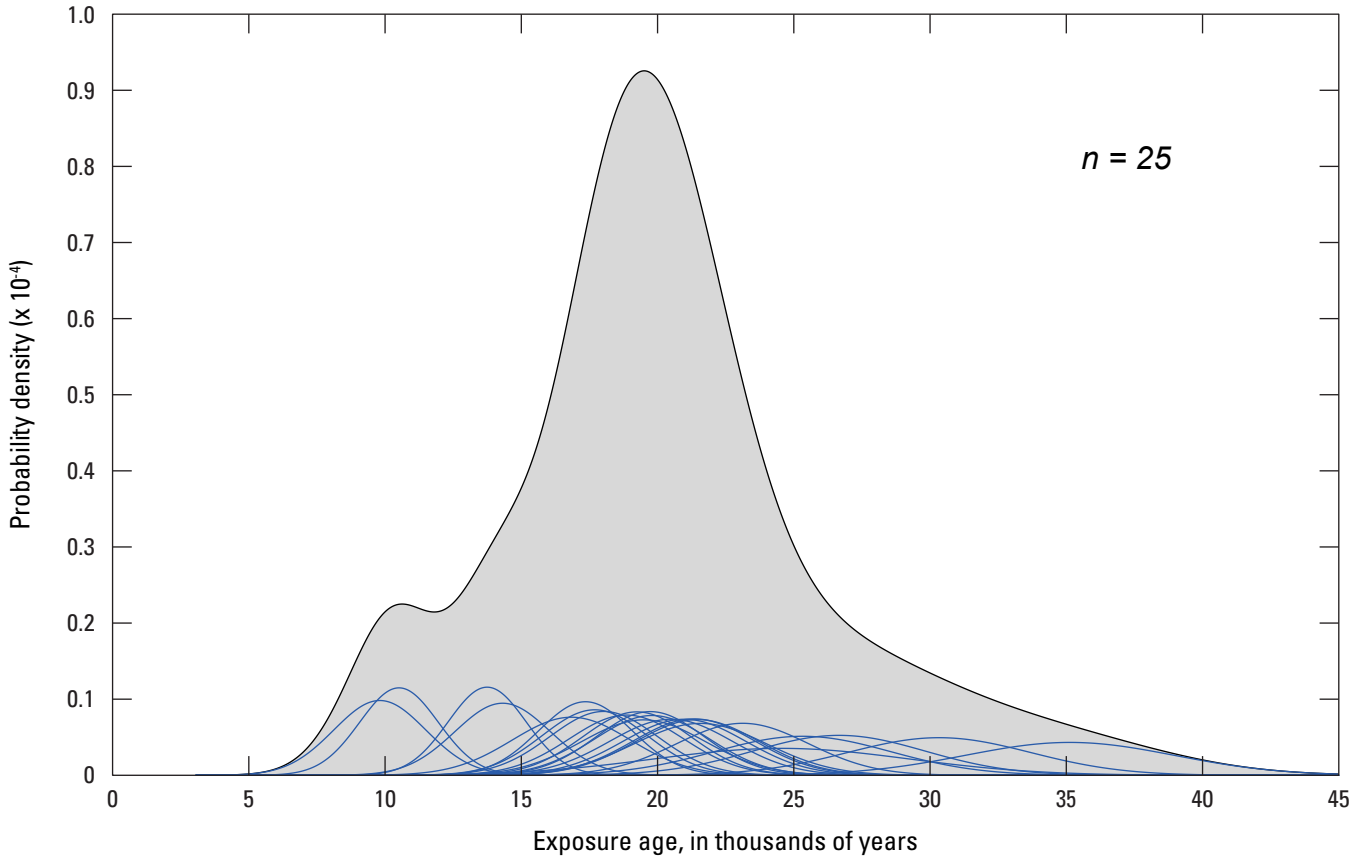

Figure 1.2. Graph showing cosmogenic ^{10}Be-exposure age data for 25 boulders from Tioga-age moraines and erratics in Yosemite National Park; sample localities shown in figure 8. Each blue line represents probability density function for one exposure age and its associated external uncertainty. Gray-shaded area represents cumulative probability density function for all ages (in other words, sum of each blue line). Boulder-exposure ages show considerable scatter, likely owing both to inherited ^{10}Be from exposure before moraine deposition and to moraine degradation. Nevertheless, mean exposure age of approximately 19,000 years (represented by peak in gray-shaded area) matches previous timing estimates of maximum position of Last Glacial Maximum (Tioga-age) glaciers in Sierra Nevada and elsewhere.

References Cited

Applegate, P.J., Urban, N.M., Laabs, B.J.C., Keller, K., and Alley, R.B., 2010, Modeling the statistical distributions of cosmogenic exposure dates from moraines: Geoscientific Model Development, v. 3, no. 1, p. 293–307.

Balco, G., Stone, J.O., Lifton, N.A., and Dunai, T.J., 2008, A complete and easily accessible means of calculating surface exposure ages or erosion rates from ^{10}Be and ^{26}Al measurements: Quaternary Geochronology, v. 3, no. 3, p. 174–195, https://doi.org/10.1016/j.quageo.2007.12.001.

Bierman, P., and Gillespie, A., 1991, Range fires—A significant factor in exposure-age determination and geomorphic surface evolution: Geology, v. 19, no. 6, p. 641–644, https://doi.org/10.1130/0091-7613(1991)019<0641:RFASFI>2.3.CO;2.

Gosse, J.C., and Phillips, F.M., 2001, Terrestrial in situ cosmogenic nuclides—Theory and application: Quaternary Science Reviews, v. 20, no. 14, p. 1475–1560, https://doi.org/10.1016/S0277-3791(00)00171-2.

Hallet, B., and Putkonen, J., 1994, Surface dating of dynamic landforms—Young boulders on aging moraines: Science, v. 265, no. 5174, p. 937–940, https://doi.org/10.1126/science.265.5174.937.

Heisinger, B., Lal, D., Jull, A.J.T., Kubik, P., Ivy-Ochs, S., Knie, K., and Nolte, E., 2002a, Production of selected cosmogenic radionuclides by muons—2. Capture of negative muons: Earth and Planetary Science Letters, v. 200, nos. 3–4, p. 357–369, https://doi.org/10.1016/S0012-821X(02)00641-6.

Heisinger, B., Lal, D., Jull, A.J.T., Kubik, P., Ivy-Ochs, S., Neumaier, S., Knie, K., Lazarev, V., and Nolte, E., 2002b, Production of selected cosmogenic radionuclides by muons—1. Fast muons: Earth and Planetary Science Letters, v. 200, nos. 3–4, p. 345–355, https://doi.org/10.1016/S0012-821X(02)00640-4.

Heyman, J., Applegate, P.J., Blomdin, R., Gribenski, N., Harbor, J.M., and Stroeven, A.P., 2016, Boulder height–exposure age relationships from a global glacial ^{10}Be compilation: Quaternary Geochronology, v. 34, p. 1–11, https://doi.org/10.1016/j.quageo.2016.03.002.

Heyman, J., Stroeven, A.P., Harbor, J.M., and Caffee, M.W., 2011, Too young or too old—Evaluating cosmogenic exposure dating based on an analysis of compiled boulder exposure ages: Earth and Planetary Science Letters, v. 302, nos. 1–2, p. 71–80, https://doi.org/10.1016/j.epsl.2010.11.040.

Kohl, C.P., and Nishiizumi, K., 1992, Chemical isolation of quartz for measurement of in-situ-produced cosmogenic nuclides: Geochimica et Cosmochimica Acta, v. 56, no. 9, p. 3583–3587, https://doi.org/10.1016/0016-7037(92)90401-4.

Lal, D., 1991, Cosmic ray labeling of erosion surfaces—In situ nuclide production rates and erosion models: Earth and Planetary Science Letters, v. 104, nos. 2–4, p. 424–439, https://doi.org/10.1016/0012-821X(91)90220-C.

Matthes, F.E., 1930, Geologic history of the Yosemite Valley: U.S. Geological Survey Professional Paper 160, 137 p., https://pubs.er.usgs.gov/publication/pp160.

Nishiizumi, K., Imamura, M., Caffee, M.W., Southon, J.R., Finkel, R.C., and McAninch, J., 2007, Absolute calibration of ^{10}Be AMS standards: Nuclear Instruments and Methods in Physics Research Section B—Beam interactions with materials and atoms, v. 258, no. 2, p. 403–413, https://doi.org/10.1016/j.nimb.2007.01.297.

Putkonen, J., and O'Neal, M., 2006, Degradation of unconsolidated Quaternary landforms in the western North America: Geomorphology, v. 75, nos. 3–4, p. 408–419, https://doi.org/10.1016/j.geomorph.2005.07.024.

Putkonen, J., and Swanson, T., 2003, Accuracy of cosmogenic ages for moraines: Quaternary Research, v. 59, no. 2, p. 255–261, https://doi.org/10.1016/S0033-5894(03)00006-1.

Putnam, R.L., Stock, G.M., Glazner, A.F., Bartley, J.M., and Coleman, D.S., 2013, Granite, glaciers, and rockfall in Yosemite Valley, California, *in* Putirka, K., ed., Geologic excursions from Fresno, California, and the central valley—A tour of California's iconic geology: Geological Society of America Field Guide 32, p. 13–35.

Small, E.E., Anderson, R.S., Repka, J.L., and Finkel, R., 1997, Erosion rates of alpine bedrock summit surfaces deduced from in situ ^{10}Be and ^{26}Al: Earth and Planetary Science Letters, v. 150, nos. 3–4, p. 413–425, https://doi.org/10.1016/S0012-821X(97)00092-7.

Stock, G.M., Anderson, R.S., and Finkel, R.C., 2005, Rates of erosion and topographic evolution of the Sierra Nevada, California, inferred from cosmogenic ^{26}Al and ^{10}Be concentrations: Earth Surface Processes and Landforms, v. 30, no. 8, p. 985–1006, https://doi.org/10.1002/esp.1258.

Stock, G.M., and Uhrhammer, R.A., 2010, Catastrophic rock avalanche 3600 years BP from El Capitan, Yosemite Valley, California: Earth Surface Processes and Landforms, v. 35, no. 8, p. 941–951, https://doi.org/10.1002/esp.1982.

Stone, J.O., 2000, Air pressure and cosmogenic isotope production: Journal of Geophysical Research—Solid Earth, v. 105, no. B10, p. 23,753–23,759, https://doi.org/10.1029/2000JB900181.

Table 1.1. Analytical results of terrestrial cosmogenic-nuclide beryllium-10 (^{10}Be) geochronology of moraine boulders in Yosemite National Park.

[Abbreviations: amsl, above mean sea level; cm, centimeter(s); g, gram(s); g^{-1}, per gram; g/cm^3, gram(s) per cubic centimeter; ka, thousand years old; m, meter(s); mg, milligram(s); σ, standard deviation; SiO_2, silicon dioxide; yr^{-1}, per year]

Sample	Location	UTM E[1]	UTM N[1]	Elevation (m amsl)	Sample thickness[1] (cm)	^{10}Be Production rate (atoms g^{-1} yr^{-1})		Shielding factor[2]	Mass quartz[3] (g)	Be carrier (mg)	^{10}Be/^{9}Be[4,5] ($\times10^{-15}$)	^{10}Be concentration[5,6,7] (10^4 atoms g^{-1} SiO_2)	Exposure age[5,8,9] (ka)
						Spallation[10]	Muons[11]						
Pre–Tioga-age moraines													
TCN-LL-2	South of Laurel Lake	255084	4208332	1,956	3.5	18.02	0.338	0.9997	18.96	0.38	1,729±42.98	231.56±7.39	Saturated
TCN-LL-5	South of Laurel Lake	255611	4207727	1,983	3	18.44	0.342	0.9999	59.96	0.38	5,334±139.8	225.89±7.44	Saturated
TCN-LL-9	Laurel Lake	254781	4209085	1,982	2.5	18.45	0.342	0.9969	33.25	0.38	2,152.0±88.4	164.34±7.51	227.8±95.7
TCN-LL-14	Laurel Lake	255379	4209689	2,024	2.5	19.05	0.347	0.9999	41.11	0.38	3,398.0±138.0	209.88±9.50	Saturated
TCN-HL-6	Harden Lake	264606	4197389	2,291	2.5	22.72	0.376	0.9996	35.14	0.38	3,945±123.2	285.07±10.57	Saturated
TCS-CWC-1	Cottonwood Creek	253778	4196518	1,830	2.5	16.61	0.327	0.9996	41.16	0.38	2,710±76.36	167.18±5.78	555.8±332.2
TBD-1	Turtleback Dome	261485	4177453	1,603	1.5	14.19	0.305	0.9984	62.09	0.37	4,051±104.2	161.31±5.26	Saturated
Tioga-age moraines													
TCN-LL-6	North of Hetch Hetchy Valley	255220	4206884	1,919	2	17.75	0.336	0.9978	14.22	0.38	225.8±14.99	40.32±2.79	25.39±3.24
TCS-CWC-2	Cottonwood Creek	253699	4197375	1,712	2	15.35	0.315	0.9995	40.32	0.38	319.10±11.97	20.10±0.85	13.78±1.44
TCS-1	Mather (“Camp Mather”)	248465	4196924	1,409	2	12.33	0.286	0.9996	8.91	0.37	66.91±4.65	18.57±1.35	14.35±1.76
TCS-2	Mather (“Camp Mather”)	245760	4196019	1,313	3	11.36	0.277	0.9968	18.17	0.37	174.6±7.22	23.75±1.09	20.55±2.25
TCS-TA-2	Mather (“Camp Mather”)	248724	4196472	1,378	3	11.96	0.283	0.9999	61.45	0.36	669.7±30.62	26.22±1.31	21.62±2.44
TCS-TA-3	Mather (“Camp Mather”)	248792	4197258	1,391	3	12.07	0.284	0.9994	40.17	0.36	334.20±14.28	20.01±0.94	17.74±1.93
BM-1	Bridalveil Moraine	265713	4177906	1,209	6	9.61	0.266	0.9377	37.68	0.3	205.10±19.22	10.91±1.05	10.54±1.44
BM-2	Bridalveil Moraine	265757	4177830	1,204	4	9.73	0.267	0.9377	58.87	0.38	598±30.15	25.79±1.40	26.73±3.17
BM-3	Bridalveil Moraine	265806	4178006	1,208	1.5	9.91	0.269	0.9318	9.85	0.3	51.52±7.03	10.48±1.45	9.83±1.69
BM-4	Bridalveil Moraine	265824	4177706	1,186	2	9.76	0.266	0.937	40.11	0.38	272.10±12.46	17.23±0.86	18.91±2.10
ECM-1[12]	El Capitan Moraine	266998	4178351	1,215	1.2	9.52	0.27	0.8884	20.25	0.3	237.4±33.52	23.50±3.35	24.61±4.70
ECM-2[12]	El Capitan Moraine	266998	4178345	1,216	2	9.46	0.269	0.8884	55.71	0.3	535.00±18.68	19.25±0.8	19.85±2.12
ECM-3[12]	El Capitan Moraine	266973	4178384	1,216	4	9.43	0.268	0.9001	43.37	0.3	359.30±27.63	16.60±1.32	16.88±2.18
LYC-1	Lower part of Yosemite Creek	271103	4183844	2,196	2.5	21.24	0.365	0.9987	19.06	0.3	428.39±14.91	45.05±1.81	21.04±2.26

Table 1.1. Analytical results of terrestrial cosmogenic-nuclide beryllium-10 (^{10}Be) geochronology of moraine boulders in Yosemite National Park—Continued.

[Abbreviations: amsl, above mean sea level; cm, centimeter(s); g, gram(s); g^{-1}, per gram; g/cm^3, gram(s) per cubic centimeter; ka, thousand years old; m, meter(s); mg, milligram(s); σ, standard deviation; SiO_2, silicon dioxide; yr^{-1}, per year]

Sample	Location	UTM E[1]	UTM N[1]	Elevation (m amsl)	Sample thickness[1] (cm)	^{10}Be Production rate (atoms g^{-1} yr^{-1})		Shielding factor[2]	Mass quartz[3] (g)	Be carrier (mg)	^{10}Be/^{9}Be[4,5] ($\times10^{-15}$)	^{10}Be concentration[5,6,7] (10^4 atoms g^{-1} SiO_2)	Exposure age[5,8,9] (ka)
						Spallation[10]	Muons[11]						
Tioga-age moraines—Continued													
LYC-2	Lower part of Yosemite Creek	271110	4183788	2,192	4	20.9	0.363	0.9977	34.72	0.3	670.40±29.57	38.70±1.87	18.07±1.98
LYC-3	Lower part of Yosemite Creek	271173	4182876	2,095	1	20.07	0.357	0.9976	17.16	0.3	341.20±19.03	39.86±2.36	19.53±2.28
LYV-LC-1	Liberty Cap	276790	4178679	2,146	4.5	19.6	0.357	0.963	83.52	0.38	1,036.81±23.61	31.52±0.74	17.40±1.72
DB-1	Half Dome (Diving Board)	276102	4180282	2,283	2.5	21.85	0.375	0.9706	40.08	0.37	629.30±16.93	38.81±1.30	19.29±1.99
DB-3	Half Dome (Diving Board)	276136	4180240	2,269	3.2	21.15	0.376	0.9362	69.24	0.36	1,791.14±22.44	62.00±1.47	35.22±3.85
WSC-1	Mount Watkins (Snow Creek)	277314	4183029	2,023	1.8	18.58	0.347	0.9761	77.34	0.38	1,030.10±13.88	33.82±0.82	19.79±1.99
LYV-MD-1	Moraine Dome	280593	4180043	2,306	2.5	22.81	0.377	0.9984	49.49	0.24	1,192±67.12	38.79±2.32	18.41±2.15
LYV-MD-2	Moraine Dome	280271	4179885	2,317	2	22.99	0.379	0.9947	59.72	0.37	1,195±32.83	49.47±1.68	21.39±2.24
LYV-MD-3	Moraine Dome	279892	4179884	2,306	2.5	22.81	0.377	0.9984	56.22	0.37	1,085±26.84	47.72±1.52	23.18±2.43
LYV-MD-4	Moraine Dome	279775	4179809	2,272	0.8	22.63	0.377	0.9986	60.64	0.37	1,202±35.19	49.01±1.74	21.52±2.27
MD-PE-1	Moraine Dome	280407	4180359	2,441	1	25.23	0.396	0.9986	45.25	0.36	1,265.90±31.08	67.29±2.13	30.41±3.36

[1]Tops of all samples were exposed at boulder surface.

[2]Geometric shielding correction for topography and sample surface orientation calculated with Cosmic-Ray Produced Nuclide Systematics (CRONUS) Earth online calculator (Balco and others, 2008), version 2.0 (http://cronus.cosmogenicnuclides.rocks/2.0/).

[3]Density of 2.7 grams per cubic centimeter was used, on basis of granitic composition of samples.

[4]Isotope ratios were normalized to ^{10}Be standards prepared by Nishiizumi and others (2007), with value of 2.85×10^{12} and using ^{10}Be half-life of 1.36×10^{6} years.

[5]Uncertainties are reported at 1σ confidence level.

[6]Mean blank value of 53,540±10,845 ^{10}Be atoms (^{10}Be/^{9}Be = $3.33\times10^{-15}\pm8.74\times10^{-16}$) was used to correct for background.

[7]Propagated uncertainties include error in blank, carrier mass (1%), and counting statistics.

[8]Propagated error in model ages include 6% uncertainty in production rate of ^{10}Be and 4% uncertainty in ^{10}Be decay constant.

[9]Beryllium-10 model ages were calculated with Cosmic-Ray Produced Nuclide Systematics (CRONUS) Earth online calculator (Balco and others, 2008), version 2.0 (http://cronus.cosmogenicnuclides.rocks/2.0/).

[10]Constant (time-invariant) local production rates are based on Lal (1991) and Stone (2000).

[11]Constant (time-invariant) local production rates are based on Heisinger and others (2002a,b).

[12]Ages recalculated from data reported in Stock and Uhrhammer (2010).

Appendix 2. Field Measurements of Glacial Striation Orientations in Yosemite National Park and Vicinity

Appendix 2 is available online at https://doi.org/10.3133/sim3414.